POLITECNICO DI MILANO

Facoltà di Ingegneria Industriale e dell'Informazione

Corso di Laurea Magistrale in
Ingegneria Energetica

INTEGRATED SOLUTIONS OF HYDROGEN STORAGE MATERIALS

Relatore: Prof.ssa Elisabetta GARIBOLDI
Correlatore: Dr. Kumar PATCHIGOLLA

Tesi di Laurea di:
Riccardo DIOTTI

Matricola: 838246

Anno Accademico 2015 – 2016

To you,
Wherever you are,
And whatever lifepath you followed.

CRANFIELD UNIVERSITY

School of Energy, Environment and Agrifood
Energy Systems and Thermal Processes

MSc

Academic Year 2015 - 2016

Riccardo Diotti

Integrated solutions of hydrogen storage materials

Supervisors: Kumar Patchigolla, Alissa Cotton
September 2016

This thesis is submitted in partial fulfilment of the requirements for the degree of
MSc Energy Systems and Thermal Processes

Sommario

Lo stoccaggio di energia gioca un ruolo cardine nell'integrazione di domanda e offerta di energia, sia sul breve sia sul lungo termine, specialmente nel settore dei trasporti dove mostra il suo più elevato potenziale.

Questo progetto di tesi ha come scopo l'indagine dei correnti e nuovi materiali di stoccaggio di idrogeno ad alta capacità per applicazioni distribuite, nello specifico il settore dei trasporti. Materiali ad alta capacità di idrogeno (ad esempio gas compresso, idruri metallici e ammoniaca) e la loro abilità di stoccare idrogeno saranno valutati, così come la loro futura implementazione commerciale come mezzi di stoccaggio di idrogeno, anche paragonando le loro proprietà con il documento del US Department of Energy 'Targets for Onboard Hydrogen Storage Systems for Light-Duty Vehicles'. In particolare, il progetto di tesi studierà lo stoccaggio di idrogeno applicato ad un caso automobilistico, ovvero il rilascio di idrogeno gassoso a bordo. La conversione di ammoniaca in idrogeno puro e le sue condizioni termodinamiche saranno valutate attraverso il software MTData™ e Aspen Plus™.

I risultati del progetto suggeriscono come nessuno dei software utilizzati sia capace di modellare la reazione adeguatamente. I risultati di MTData™ confermano la tesi del potenziale dell'ammoniaca nell' economia dell'idrogeno, tuttavia la caratteristica più critica del processo rimane la fornitura del calore di reazione necessario, calcolato nella simulazione di Aspen Plus™, nelle migliori condizioni economiche e di sicurezza dell'impianto.

Parole chiave: Idrogeno, Stoccaggio, Automotive, Idruri, Ammoniaca, MTData, Aspen Plus

Abstract

Energy storage plays a cardinal part in integrating energy demand and supply, both on a short and long timeframe, especially in the transportation sector where it shows its highest potential. Hydrogen plays an important role and might be one of the most important future energy sources.

This thesis project aims at reviewing the current/new storage materials with high hydrogen storage capacity for distributed level applications i.e. transport sector. High storage capacity materials (ex. compressed gas, metal hydrides and ammonia) and their ability to store hydrogen will be critically assessed and their future implementation as commercial hydrogen storage media will be checked, also comparing their properties with the US Department of Energy 'Targets for Onboard Hydrogen Storage Systems for Light-Duty Vehicles'. In particular, the project will study the storage of hydrogen in ammonia applied to an automotive case, i.e. the on-board release of hydrogen. The conversion from ammonia to pure hydrogen and its physical conditions will be evaluated with the software MTData™ and Aspen Plus™.

The results of this project suggest that neither of the used software was able to model the real reaction properly. The MTData™ results confirm the theory on the potential of ammonia in hydrogen economy, however the most critical feature of the process remains the supply of heat to the reaction, computed in the Aspen Plus™ simulation, in the most economical and safe condition.

Keywords: Hydrogen, Hydrogen storage, Automotive, Metal Hydrides, Ammonia, MTData, Aspen Plus

Aims and Objectives

The aim of the thesis is to underline the positive features which make hydrogen an ideal fuel for the future of automotive industry, to explain the current hydrogen storage technologies and to investigate different hydrogen storage media suitable for light-vehicle automotive application, understanding the critical issues and problems to be solved. In particular, ammonia as a hydrogen storage application will be considered due to its favourable properties, as explained in Section 1.3.3.3.

In order to do so, the objectives will be:

- to perform two software-aided simulations (the first one with MTData™ and the second one with Aspen Plus™) for hydrogen release from ammonia medium;

- to compare the results of the two software programs and the crucial technological issues;

- to compare the simulations outputs with literature results.

Acknowledgements

Contents

List of Figures

List of Tables

List of Equations

Chapter 1

Introduction

1.1 Hydrogen economy

Worldwide global economies are facing a new period of concern with choices about fuel sources, new technologies and energy regulations. The development of renewable energies is apparently the only way to maintain the current lifestyle of the western countries and to ensure a sustainable development for the others.

Moreover, there is a growing apprehension regarding the sustainability of some energy-related decisions made in the past. This is due to the rapid increase in global consumption of energy per capita (72 GJ/capita in 2005 to projected 86 GJ/capita in 2030) coupled with the fast expansion of world population, which is predicted to be 8.5 billion in 2030.[1,2] According to IEA scenarios energy demand is projected to increase by more than 50% by 2030. The need for renewable, abundant, secure and environmentally benign resources is paramount.

The global rise of energy demand will coincide with a global increase of GHGs (mainly CO_2) emissions worldwide, if the energy production will remain largely conventional fuels-based. Moreover, today, a vast majority of scientists agree on the existence of a direct connection between the global rising of temperature and the increasing concentration of GHGs in the atmosphere, as can be seen in Figure 1.1.The consensus is also on the prime role of the human activities in the observed climate change since the post industrial revolution.

	Period	Rate
	Years	°C per decade
(yellow)	25	0.177±0.052
(orange)	50	0.128±0.026
(purple)	100	0.074±0.018
(red)	150	0.045±0.012

- Annual mean
- Smoothed series
- 5-95% decadal error bars
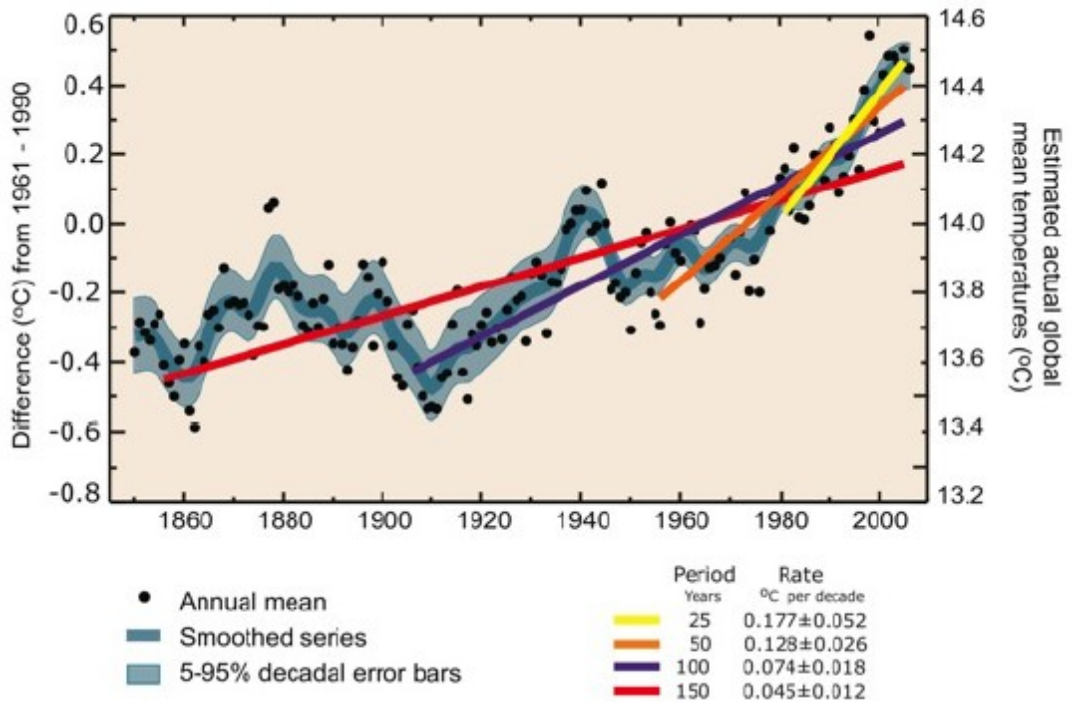
Figure 1.1: Trend of Earth surface temperature

The trend of the Earth surface temperature shown in Figure 1.1 is clearly increasing in the last 150 years, after the industrial development started increasing dramatically the burning of fossil fuels.[3]

This situation is setting off the search for alternative fuels, based on their benefits regarding mainly their environmental impact. Within this context, hydrogen production from renewable sources (photovoltaic, wind, tidal), storage and delivery have potential to play a major role in the energy system improvements of the next decades, especially in the transport sector.

For this sector, oil products comprise 93% of final energy consumption, making it the least-diversified sector.[4] Using a 25% share of Fuel Cells Electric Vehicles on roads by 2050 can grant up to 10% of total transport-related carbon emissions abatement required to shift from an IEA Energy Business As Usual scenario to a Sustainable scenario, in which the average annual global temperature increase is below 2 °C, based on the region.[5]

Hydrogen is not available in nature, but has to be anthropogenically produced in order to be technically available. Hydrogen can be considered a renewable fuel only if it is directly produced from solar light or indirectly through electricity generated by a renewable source, for example wind power or concentrating solar plants. This way hydrogen becomes also an energy storage media, hence representing a solution for the discontinuous generation that characterizes the renewable energy production technologies. Wind and solar energy are the most attractive way of exploiting this abundance: they do not emit GHGs during the conversion of energy and they are fossil fuel free.

Today 9 Mtons/yr of H_2 are produced in US alone, through steam reforming of natural gas. At present, most of the hydrogen is used in fertilizer, petroleum and chemical industries.

The interesting potential of H_2 implementation in the automotive sector is given by the fact

that just 8 kg of H_2 can cover 400-500 km in an on-board vehicle, without refilling the tank. As explained further on in this thesis, there are several ways to store hydrogen. The main obstacle for widespread application of fuel cells is the absence of sufficiently good and compact, light-weight hydrogen storage systems which are capable of delivering hydrogen gas to a fuel cell at nearly room temperature and at pressures not much higher than atmospheric pressure.[5]

1.2 Hydrogen potential in the automotive sector

Hydrogen has about the triple of the energy capacity of petrol (120 MJ/kg vs 42 MJ/kg). Indeed, hydrogen has the maximum energy to weight ratio among all fuels, as shown in Figure 1.2. However, this property is reversed on a volumetric basis, as displayed by Figure 1.3. Both the gravimetric and volumetric properties are presented in Figure 1.4.
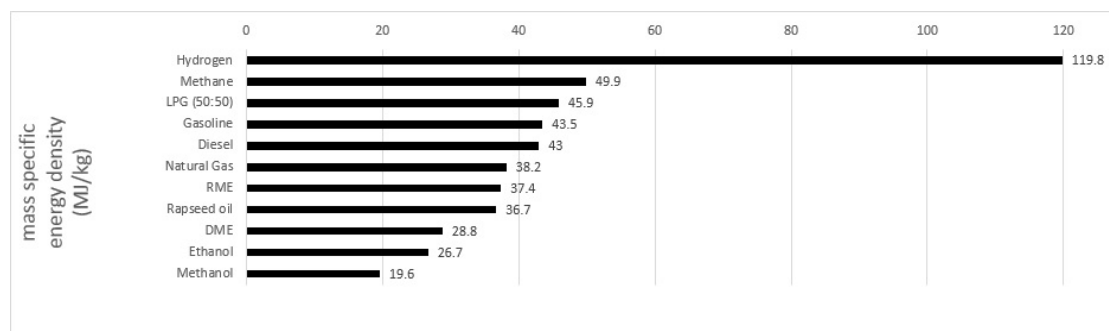
Figure 1.2: Mass specific energy densities of fuels[6]
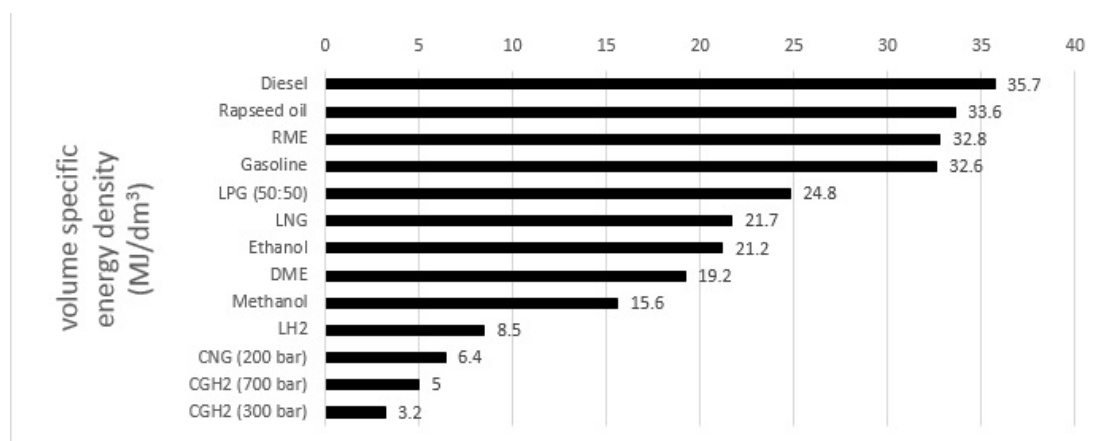
Figure 1.3: Volume specific energy densities of fuels[6]
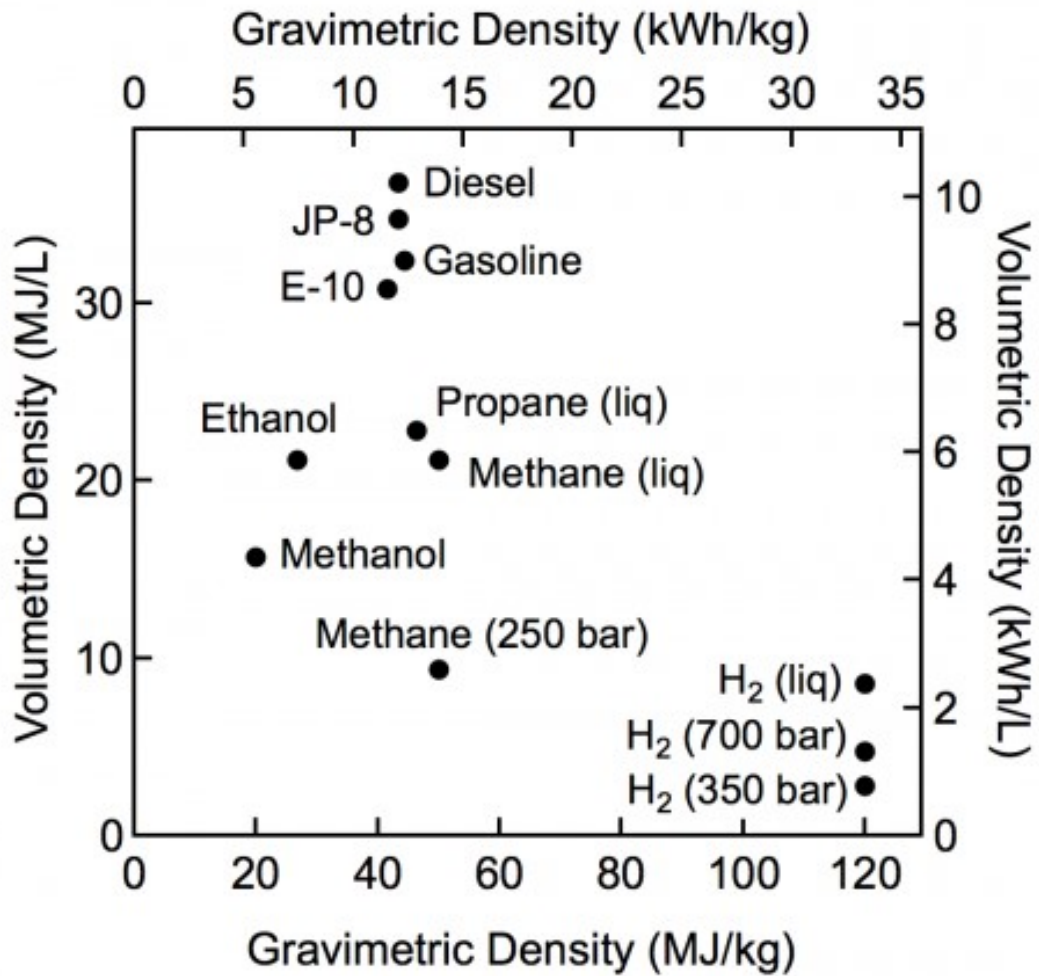
Figure 1.4: Energy properties of most diffused fuels

The minimum concentration of hydrogen required for combustion is four times higher than petrol, however the flammability range (4 vol%-75 vol%) is higher and the minimum ignition energy is lower (0.02 mJ vs 0.8 mJ) in the hydrogen case. Yet the public perception of hydrogen as a dangerous chemical.[6]

However, remarkable energy-to-weight ratio and clean emissions are the prime elements for the automotive industry which cause hydrogen to be the most desired future fuel.

The use of H_2 in vehicles is related to two main applications: hydrogen-fuelled internal combustion engines (HICE) and fuel cell electric vehicles (FCEV).

There are two key advantages with using a hydrogen powered fuel cell vehicle instead of a normal gasoline powered vehicle: the total "well-to-wheels" energy efficiency increases by a factor of three and there is no emission of greenhouse gases.

A summary of the two applications is explained by Table 1.1.

4

Passenger car	Otto-motor	Diesel-motor	PEM FC	H_2 ICE
Efficiency (NEDC)	20-35	30-40	>37	35
Investment ($/kW)	32-38	40-46	51	40-46*
Lifetime (h)	>8000	>8000	7300	>5000 20000 (Buses)

Table 1.1: Comparison of hydrogen and conventional drive trains. * – on the basis of a 70 kW engine

The lifetime of fuel cells is similar to that of other powertrain systems, for instance, the PEMFC (Proton Exchange Membrane Fuel Cell) endurance is 7300 hours under cycling status, using ternary platinum alloys and with the help of mechanical stabilisation techniques.[7,8]However, the main challenge for hydrogen storage applied to the automotive industry is competing with battery electric vehicles (BEV). The main advantage on the BEVs is the refilling/recharge time. A hydrogen vehicle is refilled at a commercial station with the replenishment timespan under 3 minutes stored in a compressed hydrogen tank (CH_2)[9] , whereas the minimum time of recharge for electric vehicles is 10 min under conditions specified in Table 1.2.

Charging time for 100 km of BEV range	Power supply	Power	Voltage	Max current
10 minutes	Direct current	120 kW	300-500 V DC	300-350 A

Table 1.2: Charging time of BEV vehicle - Tesla Motors data[10]

Since the comparison between FCEVs and BEVs has to be with range parity (500 km), the time for recharging a BEV is more than 15 times higher.
Hydrogen was discovered by British scientist Henry Cavendish in 1766, however at the beginning

it was known as *"inflammable air"*. The actual name was given by the French chemist Antoine-Laurent de Lavoisier in 1783. The first way of storing it was in gaseous form to be used as a buoyant force in aeronautical balloons. In 1783, indeed, Alexander Cesar Charles, a French scientist, used hydrogen for the first manned flight.[11]

In 1800 William Nicholson split for the first time H_2 and O_2 with electricity, discovering the electrolysis process for generating hydrogen.

In 1945 a paper by J.B.S. Haldane[12] proposed the idea of the hydrogen-based renewable energy economy, underlining the dependence of the world energy production on fossil fuels. It also pointed out the outstanding properties of hydrogen as a clean fuel.

1.2.1 Properties of hydrogen

At standard temperature and pressure it is nontoxic, colourless, tasteless, odourless and easily inflammable. Hydrogen has the simplest atomic structure being made only by a proton and an electron and it is the most diffused element in the universe (70-80 wt. % H_2 content), however it rarely occurs as a gas in its free state (1 ppm by volume in Earth's atmosphere), so that usually it is found in chemical compounds, such as hydrocarbons and water.

Despite its management issues, it has been found that hydrogen is the cleanest alternative fuel to be used both in internal combustion engines (HICE) and fuel cells (FC). Burning hydrogen generates water as a product, making it a clean fuel. In fact, as stated by Jeremy Rifkin:[13]

"There are rare moments in history when a generation of human beings are given a new gift with which to rearrange their relationship to one another and the world around them. This is such a moment... Hydrogen is a promissory note for humanity's future on Earth. Whether that promise is squandered in failed ventures and lost opportunities or used wisely on behalf of our species and our fellow creatures is up to us."

As hydrogen is formed, having an extremely short lifetime, it tends to form the hydrogen molecule H_2, as shown in Figure 1.5.
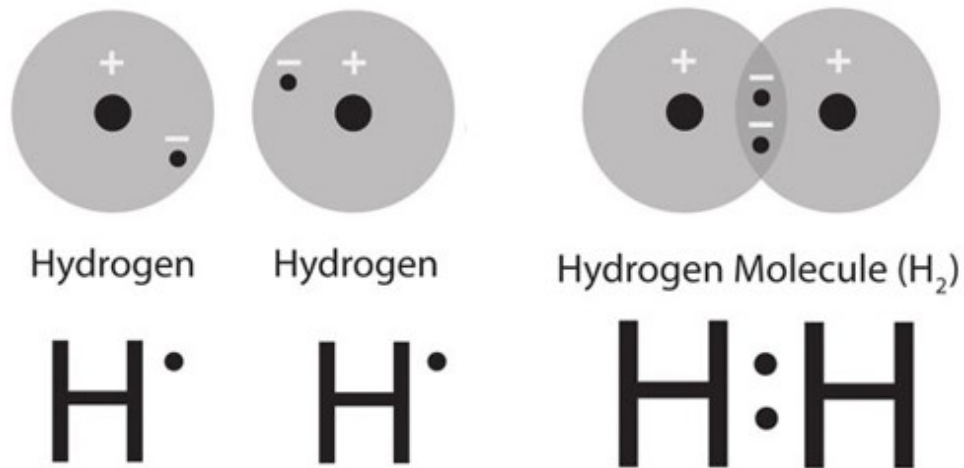
Figure 1.5: Atomic configuration of hydrogen (atoms and molecule)

Its chemical and physical properties are reported in the Table 1.3:

Parameter	Value	Unit
Molecular weight	2.016	g mol^{-1}
Lower Heating Value	120	MJ kg^{-1}
Higher Heating Value	142	MJ kg^{-1}
Triple point		
Temperature	13.8	K
Pressure	7040	Pa
Density of the liquid	0.077	g cm^{-3}
Density of the gas	0.000125	g cm^{-3}
Boiling point		
Temperature	20.3	K
Density of the gas	0.001338	g cm^{-3}
Density liquid at 20.3 K	0.071	g cm^{-3}
Liquid viscosity	11.9	µPa s
Critical point		
Temperature	33	K
Pressure	12.9	bar
Density	0.0314	g cm^{-3}
Standard properties		
Gas density (at 0 °C and 1 atm)	0.0899	g dm^{-3}
Gas viscosity (at 0 °C and 1 atm)	8.9	µPa s
Specific heat capacity Cp	14.199	KJ kg^{-1} K^{-1}
Specific heat capacity Cv	10.074	KJ kg^{-1} K^{-1}
Flammability limit in oxygen	4-94	%
Flammability limit in air	4-74	%
Density solid at 4.2 K	0.089	g cm^{-3}
Auto ignition Temperature	833	K

Table 1.3: Chemical and physical hydrogen properties

Figure 1.6 represents the phase diagram for hydrogen, with gas, liquid and solid regions, as

7

well as critical triple points.
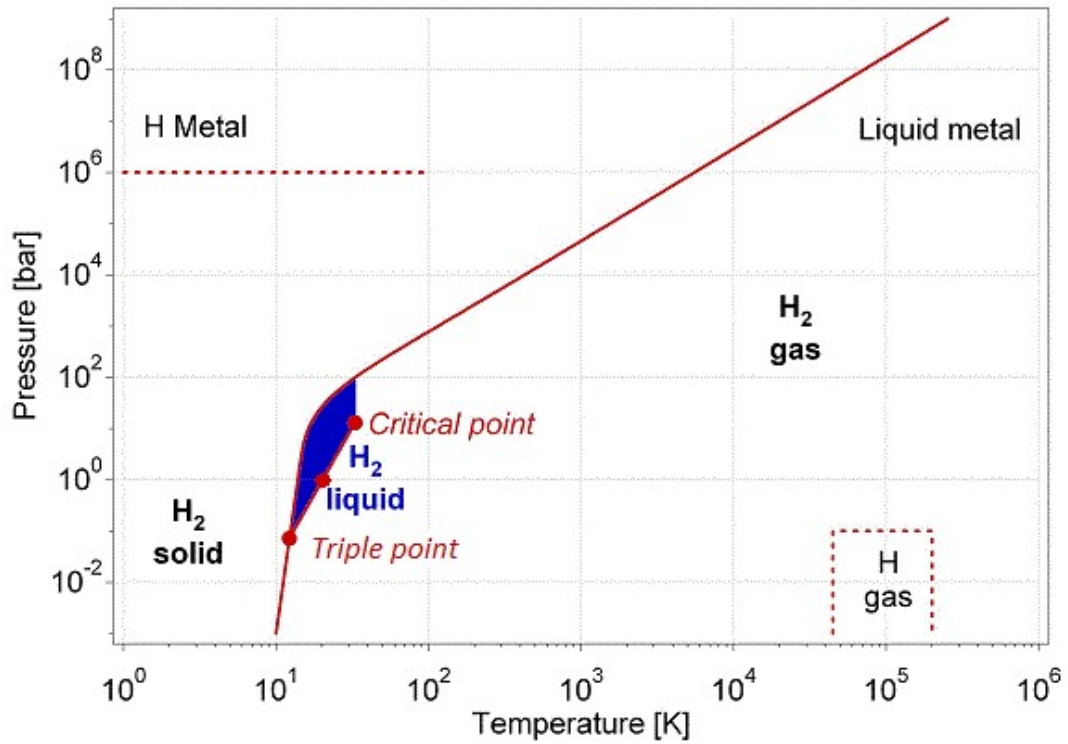
Figure 1.6: Hydrogen phase diagram[14]

The liquid phase exists only between the triple point (21.2 K) and the critical point (32 K). This means that it is not possible to liquefy the gas by applying high pressure once the hydrogen is at higher temperatures.

At ambient temperature hydrogen gas is well explained by the Van der Waals Equation 1.2.1

$$p = \frac{nRT}{V - nb} - a \left(\frac{n}{V} \right)^2 \tag{1.2.1}$$

where a and b are the Van der Waals constants equal to $0.2476 \frac{dm^2 bar}{mol^2}$ and $0.02661 \frac{dm}{mol}$, respectively.

By its applications hydrogen is comparable with other fuels, as shown Table 1.4

Fuel	Gravimetric energy density		Volumetric energy density		Flammability limits	Explosive limits	Fraction of heat in radiative form
	MJ kg^{-1}	kWh kg^{-1}	MJ dm^{-1}	kWh dm^{-1}	(vol%)	(vol%)	
Hydrogen at 200 bar and 15 °C	120	33.3	2.1	0.58			
Hydrogen liquid (20.28 K, 1 atm)	120	33.3	8.4	2.33	4-75	18.3-59.0	17-25
Methanol	19.7	5.36	15.7	4.36	6-36.5	6-36	17
Petrol	42	11.36	31.5	8.75	1-7.6	1.1-3.3	30-42
Diesel	45.3	12.58	35.5	9.86		0.6-7.5	
Kerosene	43.5	12.08	31.0	8.6		0.7-5	

Table 1.4: Most diffused fuels properties comparison[14] (room temperature)

1.2.2 Transportation

Hydrogen application in transportation started in 1807 with the Rivaz hydrogen car in Figure 1.7. The car used a single atmospherical piston internal combustion engine with a small storage system using compressed H_2.
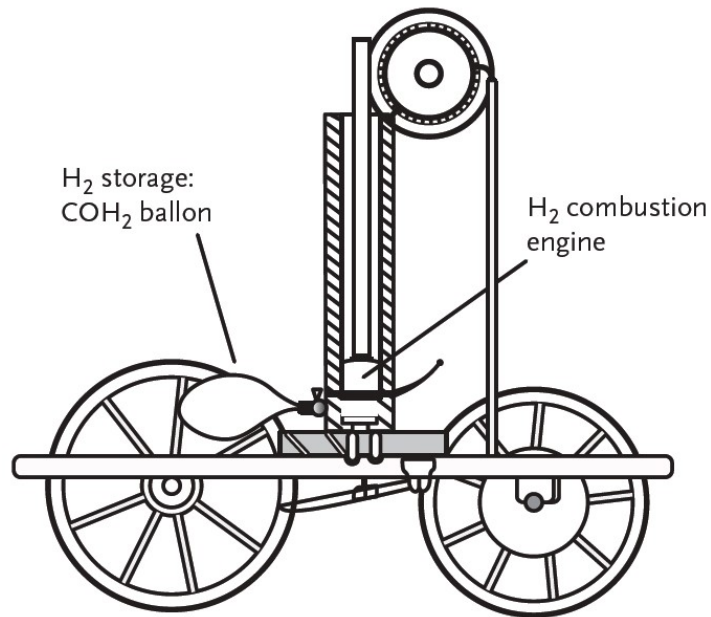
Figure 1.7: Rivaz hydrogen car

Indeed the main application of hydrogen during the twentieth century was transportation aviation with the aerostatic planes of the Zeppelin-type family and later on the Hindenburg family.

Figure 1.8: LZ 127 Graf Zeppelin

In 1931, the Hindenburg airship (Figure 1.8 was built, based on hydrogen buoyancy force. By that time hydrogen use in large dirigibles was popular in Germany and England.[15]

1.2.3   Hydrogen filling stations

Hydrogen filling stations for vehicles resemble the filling stations for natural gas. Regulations and certification are usually derived from natural gas applications, whilst hydrogen-specific regulations are being developed.[15] As the gas is filled by a pressure gradient, the reservoir pressure has to be considerably higher than the nominal tank pressure to provide a short filling time. Another important feature of the infrastructure is the filling time. Refueling of an automotive hydrogen gas tank takes a few minutes. The resulting effective energy flow can be estimated as follows: 10 kg of hydrogen contain energy of 1200 MJ. If a vessel is filled within 5 min or 300 s, the filling process corresponds to a power of $\frac{1200MJ}{300s} = 4MW$. This comes close to the values for refueling of gasoline or diesel and clearly exceeds the potential of solid storage or battery recharging.

To provide a reliable operation of the filling station, a minimum hydrogen amount of between 200 and 500 kg for a 2-day operation is required. This can only be maintained by liquified hydrogen trucking or gaseous pipeline supply. In addition to that, production of hydrogen from solar power and wind energy with reverse-electrolyses would give additional capabilities for the production of H_2 which would also be available in individual filling stations. Three examples of concrete projects were developed in the liquid hydrogen storage for automotive sector:

- The first example (Air Liquide-BP in London) was made by cryogenic tanks in which there was a technical room for operators separated from the main body of the tank for safety reasons
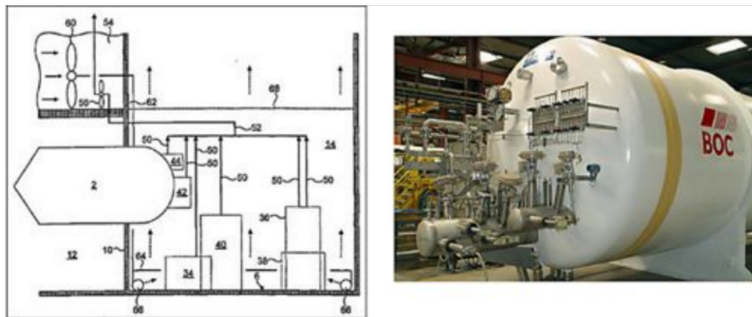
Figure 1.9: Underground storage for the LH_2 tank in the BP hydrogen refuelling station located in London. The picture of the tank is from Cryolor (tank manufacturer, subsidiary of Air Liquide), and the schematic drawing of the installation is taken from Roach (2004)

- The second example was a concept in München by Linde which comprised both LH_2 and CGH_2
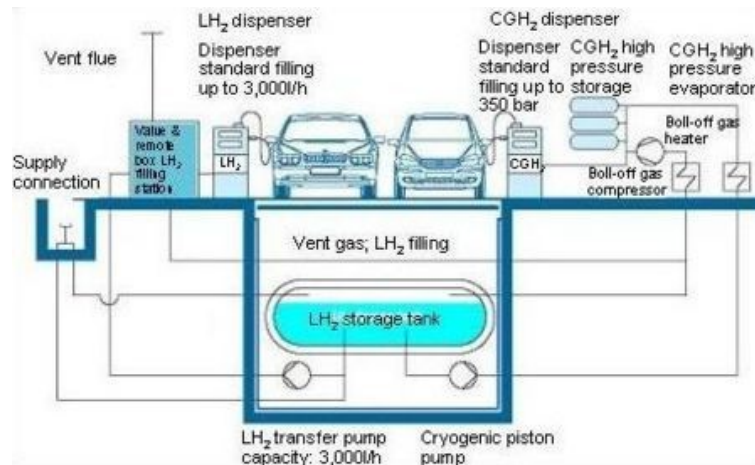
Figure 1.10: Linde concept for future hydrogen filling stations for GH_2 and LH_2 with underground storage tanks.

- The third is a concept by Air Products and Shell Hydrogen in Washington DC. All connections are accessible at ground level after the tank has been vertically slided in a cylindrical cavity. This concept applies for storage volumes from 1500 up to 9000 gallons (400 up 2400 liters) of LH_2, equivalent to 27 - 167 kg, or 320 - 1920 Nm^3 of H_2, and the boil off rate is less than 0.5% per day.

Figure 1.11: Air Products' underground LH_2 tank being installed at the Shell Hydrogen refuelling station in Washington DC in 2004.

1.3 Hydrogen storage

The storage challenge is agreeably the toughest technological issue preventing the diffusion of H_2 as an energy vector.[16, 17]

The hydrogen storage reference objectives have been fixed by the US Department of Energy,[18] as explained in Table 1.5.

Storage parameter	Units	2010	2020	Ultimate
Gravimetric capacity	g H_2 / kg system	4.5	5.5	7.5
Volumetric capacity	g H_2 / L system	28	40	70
Cost	$/gge* at pump	3-7	2-4	2-4
Operating temperature	°C	-30 to 50	-40 to 60 (sun)	-40 to 60 (sun)
Delivery temperature(min/max)	°C	-40/85	-40/85	-40/85
Cycle life (1/4 tank to full)	Cycles	1000	1500	1500
Minimum delivery pressure from system (FC/ICE)	bar (abs)	5/35	5/35	3/35
Maximum delivery pressure from system (FC/ICE)	bar (abs)	12/100	12/100	12/100
On-board efficiency	%	90	90	90
Well to power plant efficiency	%	60	60	60
System fill time (5 kg)	Min	4.2	3.3	2.5
System fill time	kg H_2/min	-	1.5	2.0
Start time to full flow (20 °C)	S	-	5	5
Start time to full flow (-20 °C)	S	-	15	15
% H_2	%	99.97	99.97	99.97
Loss of useable H	%	0.1	0.05	0.05

Table 1.5: Hydrogen storage reference objectives

* - gge stands for gasoline gallon equivalent and it is the amount of fuel it takes to equal the energy content in a liquid gallon of gasoline.
The Ultimate target in Table 1.5 is intended to make hydrogen-fueled vehicle platforms competitive across the majority of the light-duty vehicle classes (from small cars to light-duty trucks) and achieve significant market penetration.

A wide variety of vehicle types from small subcompact cars to light-duty trucks were considered in the target calculations; the fuel storage requirement varied between approximately 5 to 13 kg hydrogen, based on the corresponding vehicle type (class) and expected driving range.

The best hydrogen media should have the following features: high gravimetric and volumetric hydrogen density, fast desorption and absorption kinetics at relatively low temperatures, high reversibility in terms of number of ab-/desorption cycles, low cost, purity of the released hydrogen and safety.

Hydrogen can be stored in a number of ways:

- as a compressed gas;

- as a cryogenic liquid (Tstorage $\leq$ 32 K)

- in materials in a solid form (mainly metal hydrides)

Figure 1.12 explains the different methods used currently:
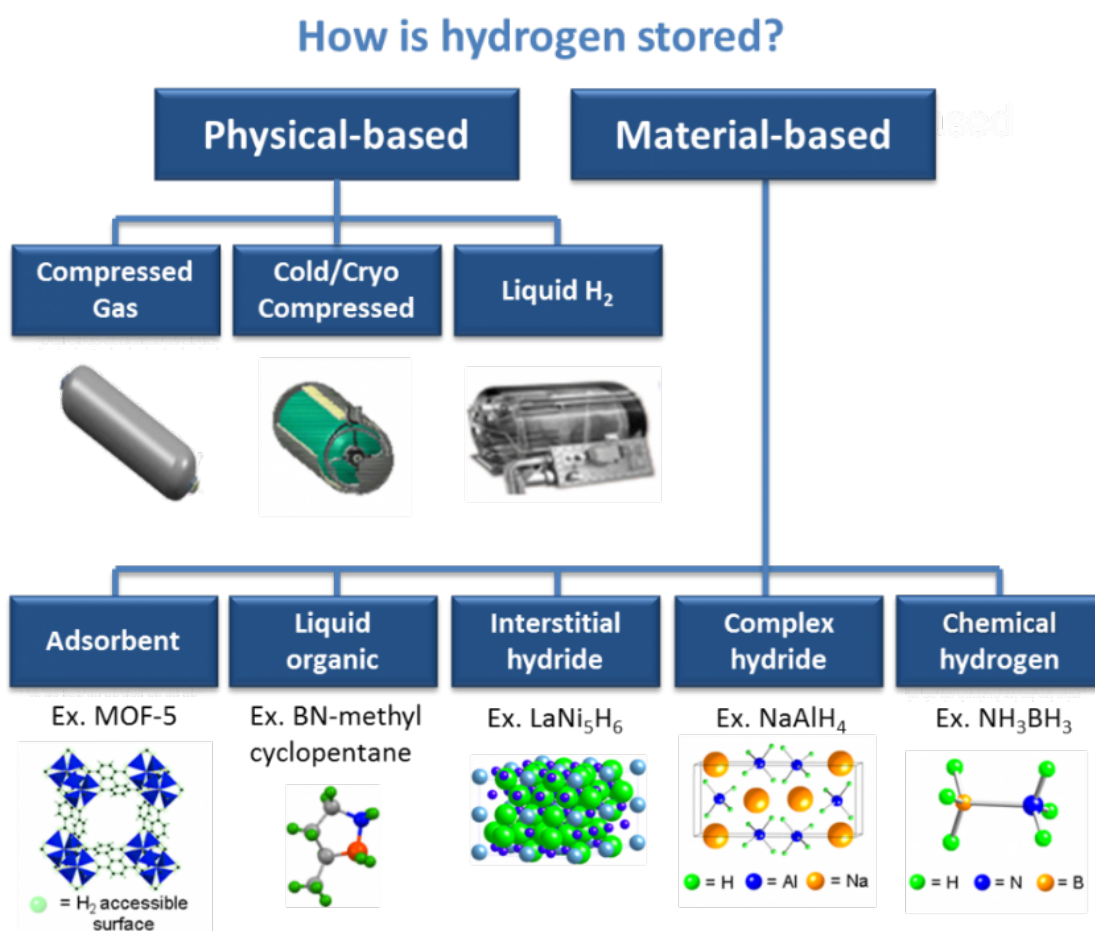
Figure 1.12: Hydrogen storage methods[18]

Cryo-adsorption is possible and is the topic of extensive research. Other adsorption approaches, zeolites, carbon materials, metal-organic frameworks, and polymers with intrinsic mi-

croporosity are areas of research.

Hirscher and coauthors[19] showed only a very low hydrogen storage capacity of about 1.0 wt% and concluded that the hydrogen storage capacity for carbon nanotubes cannot exceed 3.0 wt% at room temperature and high pressures up to 10 MPa. Indeed, the figures presented in numerous publications on carbon nanotubes and carbon materials are far from the target set by Department of Energy of USA (DOE): 6.5 wt%. Moreover, the main drawback of carbon nanotubes is the necessary use of cryogenic conditions.

1.3.1 Hydrogen compression

The gaseous density of H_2 at 1.013 bar and 15 °Cis $0.0852\frac{kg}{m^3}$,[17] which means that 1 kg of H_2 occupies $11.74m^3$, which is an unfeasible value for hydrogen storage.

One may use the adiabatic compression equation $PV^\gamma = const$ where $\gamma = \frac{c_p}{c_v}$ and add the efficiencies of the electric generator and the compressor. However, the most suitable modelling of hydrogen compression is given by the Equation 1.3.1.

$$(p + \frac{a \cdot n^2}{V^2})(V - n \cdot b) = nRT \tag{1.3.1}$$

Where $a = 24.7170\frac{L^2kPa}{mol^{-2}}$ measures the attraction of the hydrogen molecules and $b = 0.0270Lmol^{-}1$ measures the excluded volume by a mole of hydrogen. At lower pressures, the relationship is more or less proportional. At higher pressures, though, the density does not raise further in the same ratio.
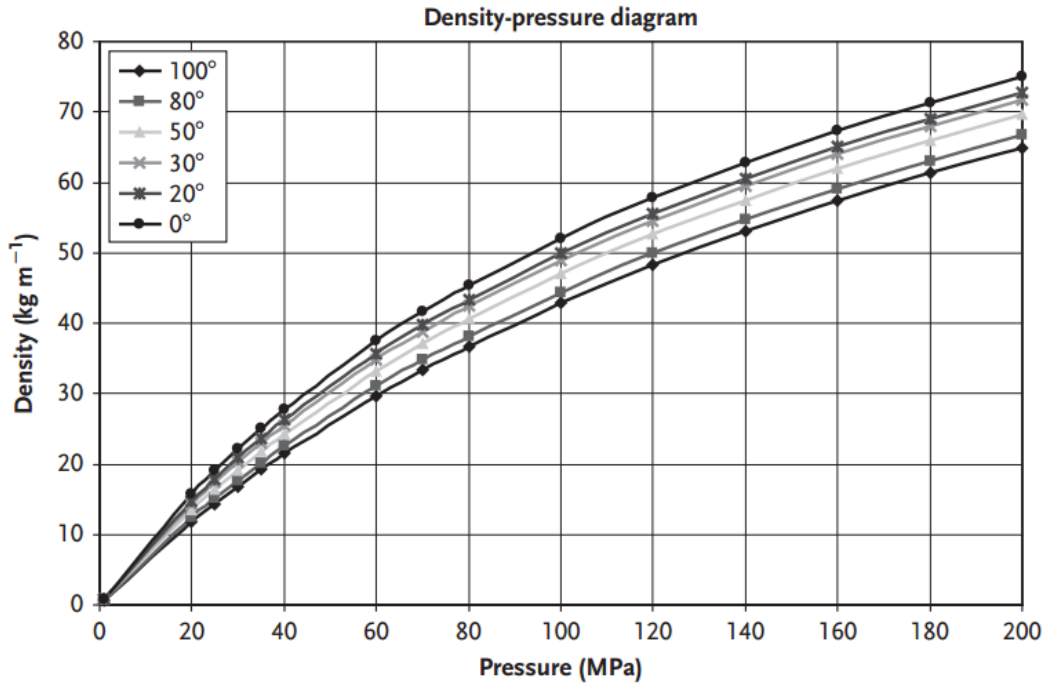
Figure 1.13: Density of compressed hydrogen as function of the pressure at different temperatures

The plot in Figure 1.13 shows that compressing hydrogen to 5,000 psi (340 atm) and 10,000 (680 atm) will need 36 MJ/kg and 47 MJ/kg. These is equal to 30 and 40% of the hydrogen low heat value (LHV), respectively. Therefore, hydrogen storage as a compressed gas is quite energy demanding.

The most common storage system is high-pressure gas cylinders, which work at a maximum pressure of 700 bar (Onboard Type IV Compressed Hydrogen Storage Systems). The correlation between the wall thickness of a cylinder capped with two hemispheres and the applied stress σ_v is and overpressure Δp given by Equation 1.3.2.

$$\frac{t_w}{d_o} = \frac{\Delta p}{2 \cdot \sigma_v + \Delta p} \tag{1.3.2}$$

where t_w is the wall thickness, d_o the outer diameter of the cylinder, Δp the overpressure.

A very simplified way to estimate the thickness is to consider the maximum stress as the material Ultimate Tensile strength, as done by Zuttel in *Materials for hydrogen storage* (2003).

The Ultimate tensile strength of materials is in the range between 50 MPa (for aluminium) to more than 1100 MPa (for steel, AISI 4130, water quenched 855 °Cor 480 °Ctemper). New lightweight composite cylinders can withstand pressures up to 80 MPa, so that H_2 can reach a volumetric density of $36 \frac{kg}{m^3}$.[20, 21]

As shown in Figure 1.14, the volumetric H_2 density raises with pressure and reaches a maximum above 1000 bar, depending on σ_v of the material. Therefore, the critical issue in pressurised gas systems is that the increase in volumetric storage density is sacrificed with the decrement of the gravimetric density.
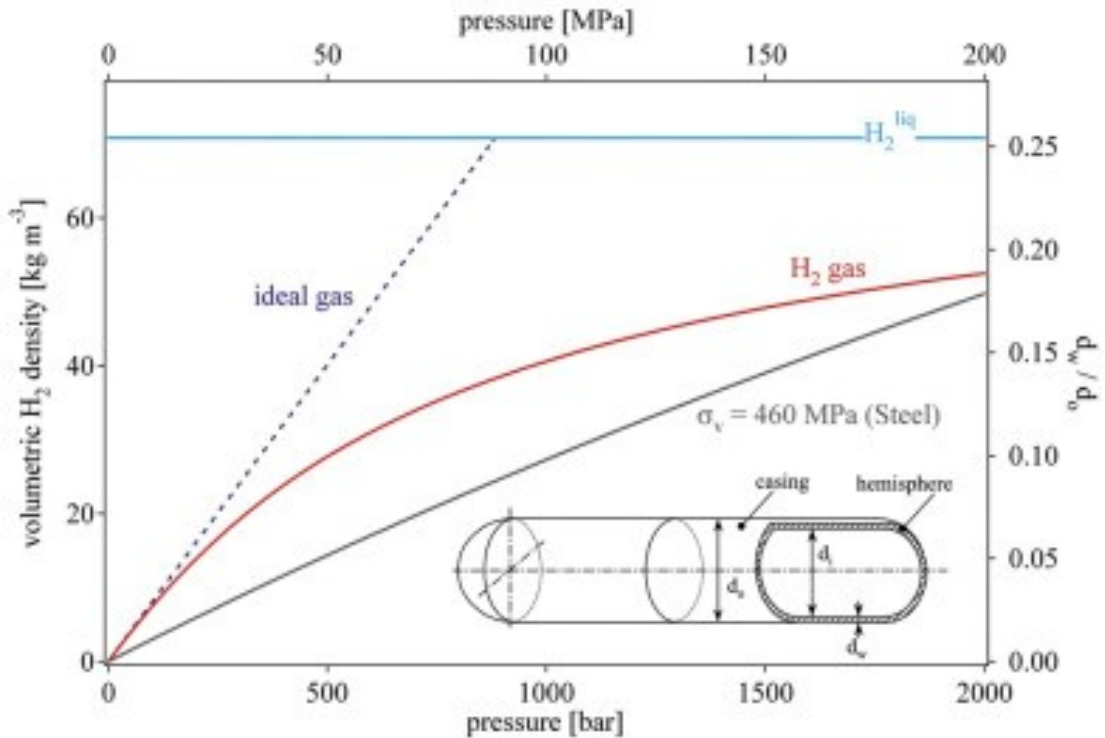
Figure 1.14: Hydrogen storage features as compressed gas

About gas compression, it is predicted that future pressure vessels will be made of three layers: an inner polymer liner, an overwrapping carbon-fiber composite (which is the stress-bearing component) and an outer layer of an aramid-material capable of withstanding mechanical and corrosion damage. Industry has set itself a target of a 110 kg, 70 MPa cylinder with a gravimetric storage density of 6 mass% and a volumetric storage density of $30 kg \cdot m^{-3}$. This relatively simple solution was already successfully tested on the market.

The ground transportation issue is mainly linked to buses for urban usage; this was mainly performed with CH_2 in cylindrical tanks sorted in racks, for example, mounted on the roof fuselage of the space frame body of buses. City buses which are run by hydrogen were launched in Germany, Japan, and UK (see Figure 1.15). However, even if the pressure inside of tanks is increased up to 600 bar the density of hydrogen is too low for automotive applications.
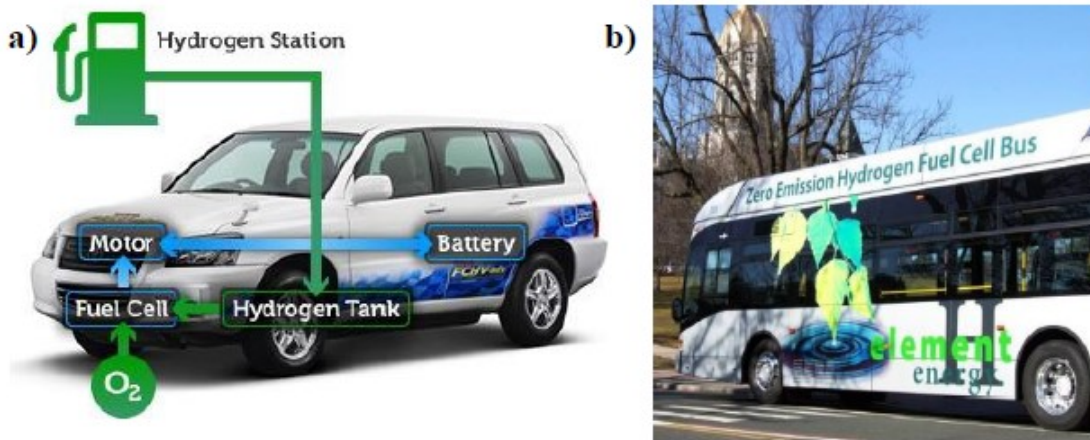
Figure 1.15: a) Schematic representation of a fuel cell vehicle; b) a city bus with a fuel cell engine and hydrogen as a fuel.

The development of new lightweight composite cylinders, capable of supporting 80 MPa, has brought their hydrogen volumetric density to $36 \frac{kg}{m^3}$, half as much as in the liquid form. Regarding this technology, it must be considered that the compression of hydrogen requires energy (reaching 80 MPa requires roughly 6-7% of the energy stored per kg) and high pressure vessels threaten the security of on-board applications and densely populated areas.

Hydrogen has a tendency to adsorb and dissociate at material surfaces, the atomic hydrogen then diffuses into the material and causes embrittlement and diffusion.

Materials suitable for hydrogen applications are mainly austenitic stainless steel and aluminum alloys. To reduce the weight, steel containers have been replaced by composite containers. With type IV containers, the liners are also made of synthetic material. Composite containers are lighter but also expensive, especially with a growing demand for carbon fibers. For automotive applications, a number of type III and type IV tank systems are available. Their characteristics in Table 1.6 show that energy densities are considerably higher and reach gravimetrically $0.055 kg_{H_2} kg^{-1} or 1.833 kWh kg^{-1}$ and volumetrically $0.026 kg_{H_2} dm^{-3} or 0.867 kWh dm^{-3}$. The costs of available tank systems vary from about 40 €per kWh of stored hydrogen energy for type III tanks for 350 bar up to about 150 €per kWh for type IV tanks for 700 bar.

Net volume [dm^3]	34	100	50	100	36	65	30	120
Type	III	III	III	III	IV	IV	IV	IV
Nominal pressure [bar]	350	350	700	700	350	350	700	700
Test pressure [bar]	525	525	1050	1050	525	525	1050	1050
Tank system weight [kg]	18	48	55	95	18	33	26	84
Tank system volume [dm^3]	50	150	80	150	60	100	60	200
H2 density [kg m^{-3}] at 25 °C	23.3	23.3	39.3	39.3	23.3	23.3	39.3	39.3
H2 content [Nm^3]	8.83	26	21.84	43.69	9.35	16.96	13.5	51.7
H2 content [kg]	0.79	2.33	1.96	3.83	0.84	1.52	1.21	4.65
Grav. H2 content [kg$_{H2}$ kg^{-1}]	0.044	0.049	0.036	0.041	0.047	0.047	0.047	0.055
Vol. H2 content [kg$_{H2}$ dm^{-3}]	0.016	0.016	0.025	0.026	0.014	0.015	0.021	0.023
Grav. energy density [kWh kg^{-1}]	1.467	1.633	1.200	1.367	1.567	1.567	1.567	1.833
Vol. energy density [kWh dm^{-3}]	0.533	0.533	0.833	0.867	0.467	0.500	0.700	0.767

Table 1.6: Characteristics of commercially obtainable automotive pressure containers[17]
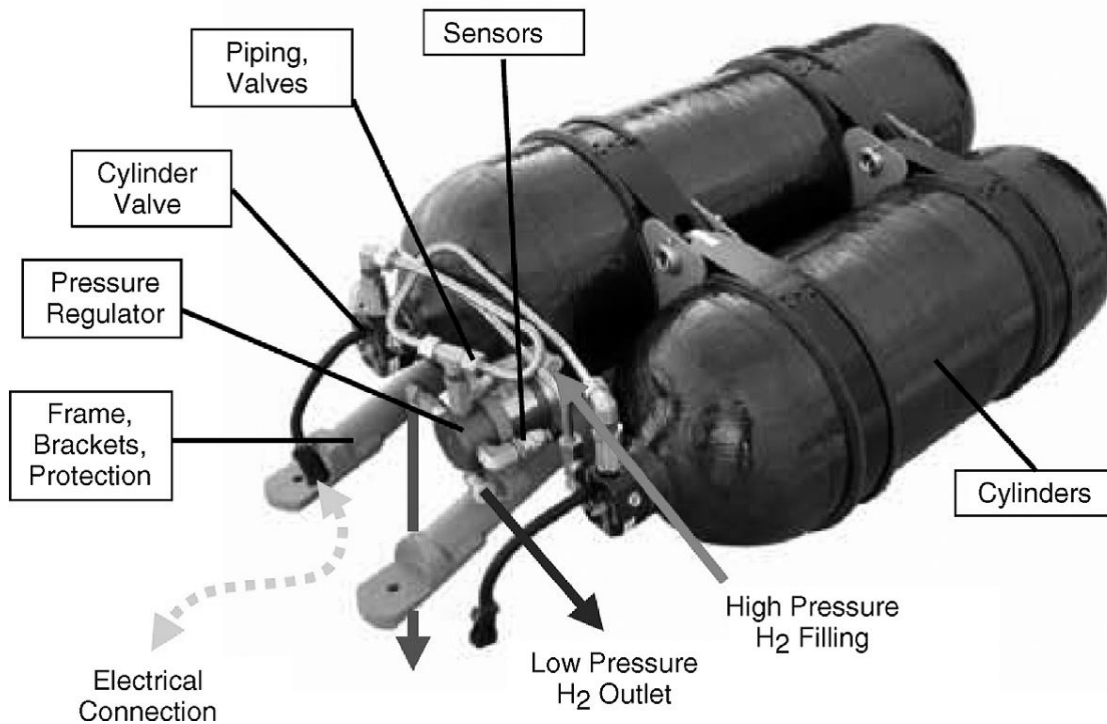
Figure 1.16: Compressed hydrogen tank for automotive application. Source Dynetek Industries Ltd.

However, this storage method leads to several drawbacks e.g. safety concerns, cost of pressurization, hydrogen embrittlement of hydrogen tank and suddenly drop of pressure during use. The most widely studied options for storing large quantities of gaseous hydrogen are underground depleted gas fields or aquifers, and caverns.

1.3.2 Hydrogen liquefaction

For cryogenic liquid hydrogen, the theoretical cooling energy expenditure is:

- 2.94 MJ/kg H_2 for gas from 298 K to 20 K

- 0.45 MJ/kg for gas to liquid at 20 K

Total: 3.40 MJ/kg from gas at 298 K to liquid at 20 K
Indeed, liquefaction involves a reverse Carnot cycle with efficiency of:

$$\eta_{reverseCarnot} = \frac{Q_{extraction}}{Q_{rejection} - Q_{extraction}} = \frac{T_2\Delta S}{T_1\Delta S - T_2\Delta S} = \frac{T_2}{T_1 - T_2} \qquad (1.3.3)$$

which for liquefaction (T1 = 298 K and T2 = 20 K) is equal to 0.0719 or 7.19%.
At standard (normal) conditions, molecular hydrogen is a mixture of about 75 vol% ortho- and 25 vol% para-hydrogen, which is called normal hydrogen. With a reduction in temperature, the content of para-hydrogen increases and reaches 100 vol% below 200 ℃. The mixture of ortho- and para-hydrogen at thermodynamic equilibrium at a certain temperature is called equilibrium

hydrogen. Para-hydrogen has a lower energy level than ortho-hydrogen, so during the liquefaction of hydrogen, additional energy has to be dissipated to convert ortho- to para-hydrogen. Moreover, one of the major issues of this storage type is boil-off leaking of liquid hydrogen.[14]

1.3.3   Hydrogen embrittlement

Embrittlement is the loss of ductility, impact energy and crack growth resistance of a material caused by hydrogen in combination with stress, either external or internal. The hydrogen-environment embrittlement of metals and alloys is observed in gaseous hydrogen, particularly in high-purity, high-pressure hydrogen at room temperature.[22] It could occur at very low temperature with a H concentration gradient. Once H atoms are inside the metal cavities they could recombine into H_2 and generating an internal pressure which can cause cracking (Hydrogen-Induced Cracking or HIC).
Materials that are most vulnerable include high-strength steels,[23] titanium, aluminium alloys and electrolytic tough pitch copper, although the FCC structure makes the transport of hydrogen in aluminium slower than in the high-strength steels.[24,25]
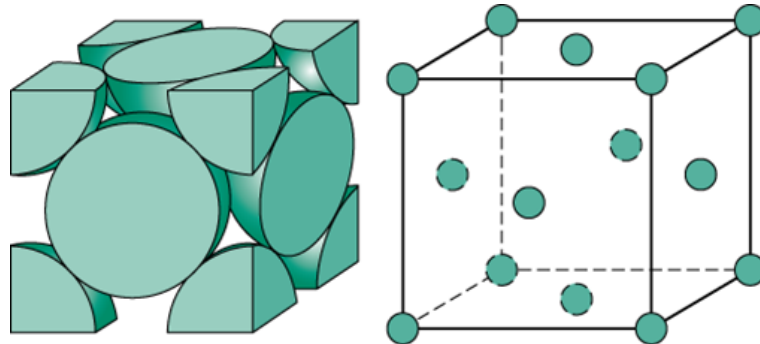
Figure 1.17: Face-centered cubic (FCC) system (atomic packing factor = 0.74)

Hydrogen embrittlement is a result of hydrogen concentration builds up in the metal that with time will form blisters and cracks at internal interphases such as grain boundaries, inclusions and second phase particles eventually lead to failure. Hydrogen embrittlement is similar to stress-corrosion in that a normally ductile metal experiences brittle fracture when exposed to both a tensile stress and hydrogen resulting from metal dissolution in a corrosive atmosphere. Hydrogen embrittlement does not require any particular chemical reaction of H with other compounds inside the metal, since experimental evidences shown that its atomic form is responsible of embrittling phenomena.
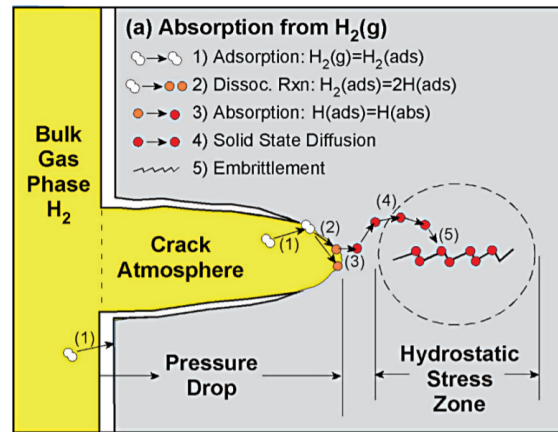
Figure 1.18: Hydrogen embrittlement mechanism[22]

Figure 1.24 shows the hydrogen embrittlement phenomenon in H_2 rich atmosphere as the one generated in molecular H_2 gaseous or liquid storage. There are five phases (adsorption, diffusion, absorption, solid state diffusion and embrittlement) which can take up to several areas to occur in which H_2 leads to cracking of the metal. The diffusion phase has been studied in the past starting from the simple Fick's law model to more and more complex approaches.

Figure 1.19: Hydrogen embrittlement and failure of a hard chromium-plated chain conveyor bolt.

Hydrogen deeply affect the behaviour of the materials increasing crack growth up to 40 times[24] and reducing the numbers of cycles to failure.[25] Moreover, there is a clear evidence that hydrogen embrittlement is related to kinetics and diffusion of H through the metal lattice. Regarding steel, an important remark should be done if considering either FCC or BCC structure.
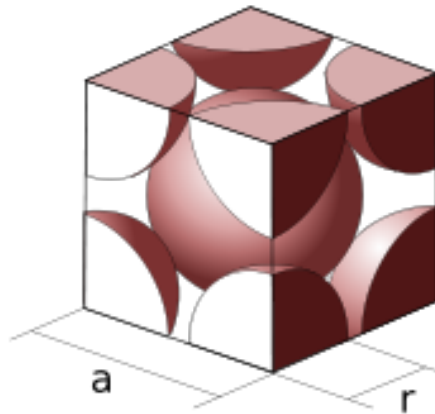
Figure 1.20: Body-centered cubic (BCC) system (atomic packing factor = 0.68)

BCC structure, typical of ferrite, has small holes between the metal atoms and can contain (solute) less hydrogen than FCC (typical of austenite); on the other hand in ferrite the channels between the holes are wide and hydrogen diffusion is higher than austenite.[23] Consequently, it usually takes longer times (years rather than days) for austenitic materials to become embrittled by hydrogen. Indeed, BCC and HCP structured materials are more susceptible compared to FCC structured materials.
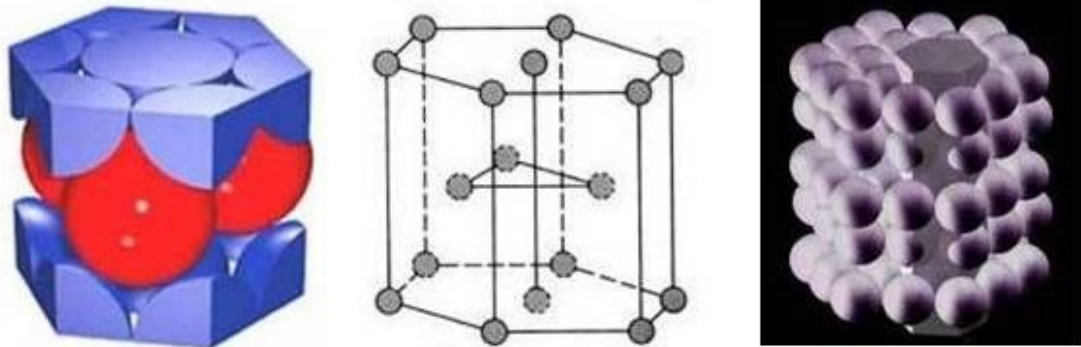
Figure 1.21: Hexagonal closed-packed (HCP) system (atomic packing factor = 0.74)

Hence regarding hydrogen-induced stress cracking, ferritic, martensitic and duplex stainless steel are more vulnerable than austenitic grades.[26] According to the times of hydrogen embrittlement phenomenon, austenitic stainless steel and aluminium and its alloys can be considered almost immune to hydrogen embrittlement most of the times.[28]

22

1.3.4 Solid state and chemicals hydrogen storage

In recent years hydrogen storage in solid state was considered to be worthy of note due to the potential properties mainly of metal hydrides. Furthermore, even chemicals containing hydrogen showed interesting features. In the following sections their advantages and drawbacks will be analised.

One of the challenges of CHS materials is addressing the energy barriers required to break the chemical bonds and release the hydrogen.

An ideal hydrogen storage material can be dehydrogenated onboard a vehicle or device without using large amounts of energy to initiate the hydrogen release reaction while being regenerated without excessive energy addition requirements. Unfortunately, achieving both of these targets with a single material has been elusive.

Regarding hydrocarbons storage, there are issues of the aromatic and heterocyclic compounds:

- cracking, ring opening, or hydrocracking (hydrogenolysis) of the aromatic hydrocarbons during the hydrogenation–dehydrogenation cycles;

- formation of strongly condensable hydrocarbons, such as formation of tars and coke which turn the substrate into a solid material that cannot be removed easily from the reaction volume these heavy products can also deactivate the homogeneous or heterogeneous catalysts.

Hydrogen storage materials could be divided into two classes depending on the mechanism of hydrogen sorption: materials where adsorption is due to physisorption or due to chemisorption. In case of physisorption, molecular hydrogen is weakly bound to the surface of the material by van der Waals or hydrogen bonds. In case of chemisorption, H_2 molecules dissociate into atomic hydrogen which is then absorbed into the bulk forming stronger ionic or covalent bonds with the material.

Physisorption

The use of physisorption-based hydrogen storage materials is being studied as a mean of transporting hydrogen gas compactly. Since this method enables hydrogen desorption at ambient temperature, the storage systems are simple and heat is generally not required for hydrogen desorption. The development of such physisorption-based hydrogen storage materials is being actively pursued. It has also been reported that materials such as carbon nanotubes, graphene based carbons, carbon nanofibers and activated carbons have shown relatively high hydrogen storage capacities. But at present, no one has successfully developed carbon materials with storage capacities high enough to be useful for practical applications.

Recent development in nanoscale engineering yielded a series of high-surface-area materials such as nanoporous scaffolds, carbon nanotubes, etc. able to absorb gas molecules on their surface by the so-called van der Walls interactions. Owing to these weak interactions, physisorption is observed only at very low temperatures, less than -170 ℃, with also low amounts of adsorbed hydrogen (around 2-4wt%)[16, 29]

Metal hydrides

The generic formation reaction of a metal hydride is shown in Equation 1.3.4.

$$M + \frac{x}{2}H_2 \rightarrow MH_x + heat \tag{1.3.4}$$

Metal hydrides can be formed by charging metals with gaseous hydrogen either in molecular or atomic form.
Figure 1.28 explains the steps of the process.
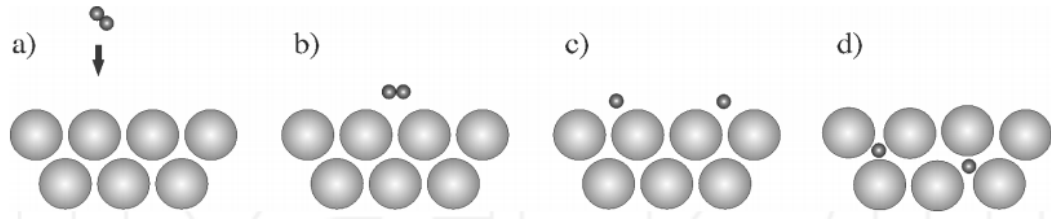
Figure 1.22: Reaction of a H_2 molecule with a storage material: a) H_2 molecule approaching the metal surface. b) Interaction of the H_2 molecule by Van der Waals forces (physisorbed state). c) Chemisorbed hydrogen after dissociation. d) Occupation of subsurface sites[14]

Hydrogen reacts at high T with the electropositive elements, i.e. the elements which are more likely to donate electrons forming ions, namely Sc, Yt, lanthanides, actinides, and members of the Ti and Va groups.[30]
However, for the purpose of this study, the main required properties include good kinetics of absorption/desorption processes, and a suitable pressure and temperature condition for that to happen. The criteria have been set to a maximum pressure of 8 bar and a maximum temperature, determined by the release of waste heat from fuel cells in PEMFCEVs, of 200-250 ℃.
According to the classification of Zuttel,[31] there are several types of metal hydrides: Interstitial hydrides, which are divided into Intermetallic compounds and Modified binary hydrides, and Complex hydrides, which are further classified into Alanates and Borohydrides.
Interstitial hydrides
They are mainly formed by binary or higher order reaction of a metal with H_2. The reaction is as described in Figure 1.28: molecular H_2 dissociates on the surface of the metal and diffuses through it as atomic hydrogen. The main aspect of these compounds is that, regarding storage purpose, some of them are too stable (they show too high pressures and too high enthalpy of reaction of hydrogen release), while some of them are too unstable (they show too low pressures and too low enthalpy of reaction of hydrogen release). Concerning mobile applications, their gravimetric capacity is relatively low ($1 - 4$ wt. % H_2) to show viable commercialisation.
Intermetallic compounds
They are formed by two metals, A and B such that: AH_x is a stable hydride and BHx is an unstable hydride. From the literature[19] it is know that the formation reaction of $A_mB_nH_z$ is as described by Equation 1.3.5 and that this compound is stable and its hydrogen release enthalpy is such that: $\Delta H_{A,release} < \Delta H_{AB,release} < \Delta H_{B,release}$. A comparison between intermetallic compounds and other forms of storage is shown in Table 1.7.

$$A_xB_y + H_z \rightarrow A_xB_yH_z \tag{1.3.5}$$

Material	H-atoms per cm³ (x 10²²)	% of weight that is hydrogen
H_2 gas 200 bar (2850 psi)	0.99	100
H_2 liquid 20 K (-253 °C)	4.2	100
H_2 solid 4.2 K (-269 °C)	5.3	100
MgH_2	6.5	7.6
Mg_2NiH_4	5.9	3.6
$FeTiH_2$	6.0	1.89
$LaNi_5H_6$	5.5	1.37

Table 1.7: Storage characteristics of pure hydrogen and some alloys

The hydrides of the transition metals have metallic character and they are good conductors.
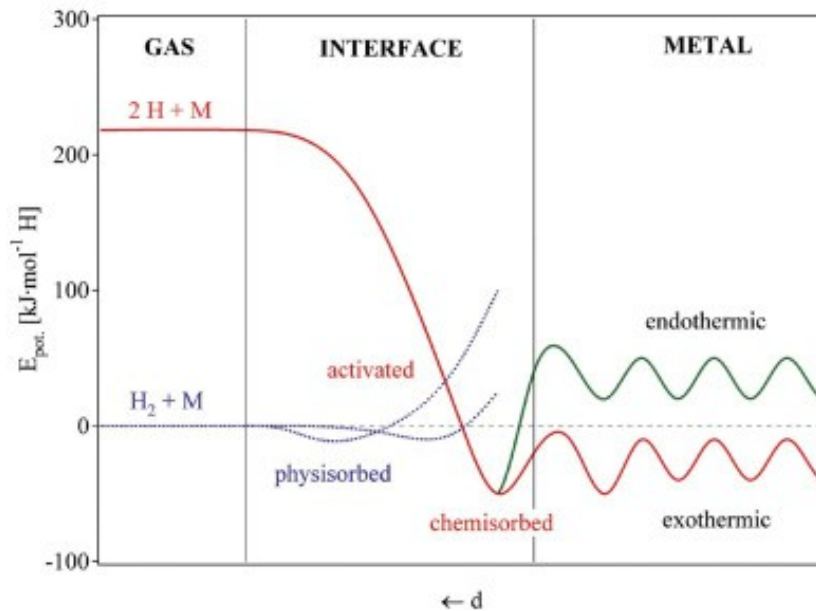
Figure 1.23: Intermetallic compounds gas-metal interactions[29]

Without any other interaction, the energy of molecular hydrogen and atomic hydrogen are divided by the dissociation energy ($H_2 \rightarrow 2H$, $E_{Diss} = 435.99 kJmol^{-1}$). In Figure 1.23, the flat minimum in the H_2 + M curve corresponds to physisorbed H_2 with energy Ephys, while the deep minimum in the 2H + M curve illustrates chemisorbed and dissociated H. As the molecule approaches to the metal surface, the Van der Waals force rises generating physisorption ($E_{Phys} \approx 10 kJmol^{-1}$). As the hydrogen comes closer to the surface, it has overcome the activation barrier, which depends on the surface elements utilized. The hydrogen shift to the chemisorbed phase ($E_{Chem} \approx 50 kJmol^{-1}$). The chemisorbed hydrogen atoms have a high surface mobility, can interact with each other, and form surface phases at sufficiently high coverage. Finally, the chemisorbed hydrogen atom can diffuse through the metal.[30]

After dissociation on the metal surface, the hydrogen atoms have to diffuse into the bulk metal and they can form there different structures and configurations, see Figure 1.24.[30]
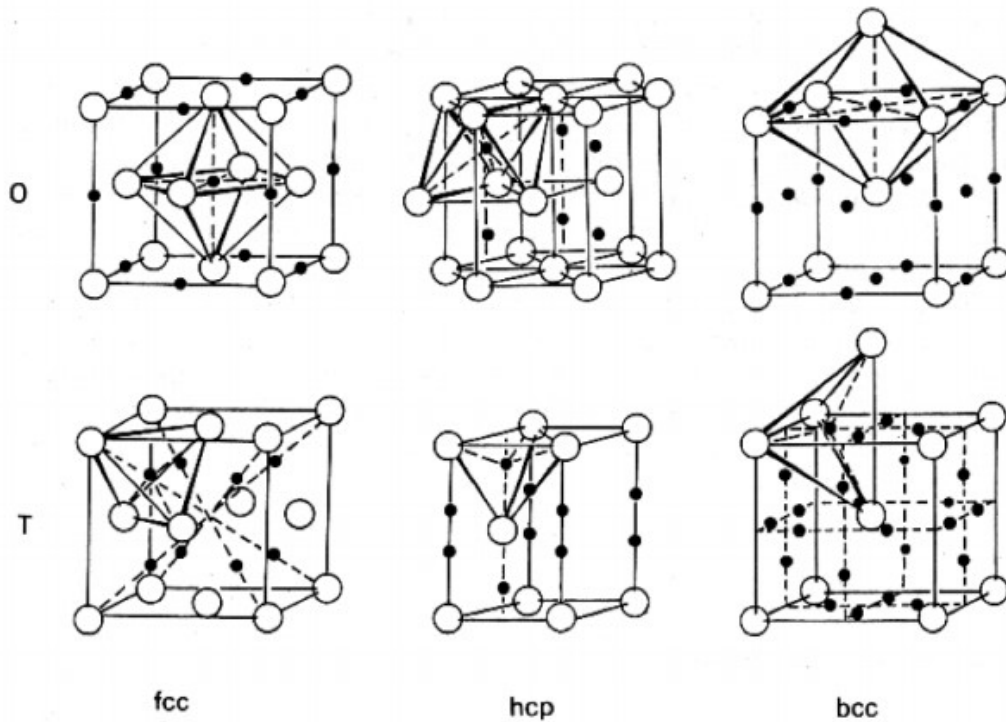
Figure 1.24: Octahedral (O) and tetrahedral (T) interstitial sites in fcc-, hcp- and bcc-type metals. (Fukai, 1993)[21]

A typical reversible hydride shows absorption and desorption *pressure-composition (P-C) isotherms*. This measurement is computed keeping an alloy sample at constant T while correctly checking the amount of hydrogen sorbed and the p of the sorption, see Figure 1.25. The reaction in this case follows the Van't Hoff Equation 1.3.6.

$$ln(\frac{p_{eq}}{p_{eq}^0}) = \frac{\Delta H}{RT} - \frac{\Delta S}{R} \tag{1.3.6}$$

where p_eq is the equilibrium pressure, p_{eq}^0 is the reference pressure and R is the gas constant.
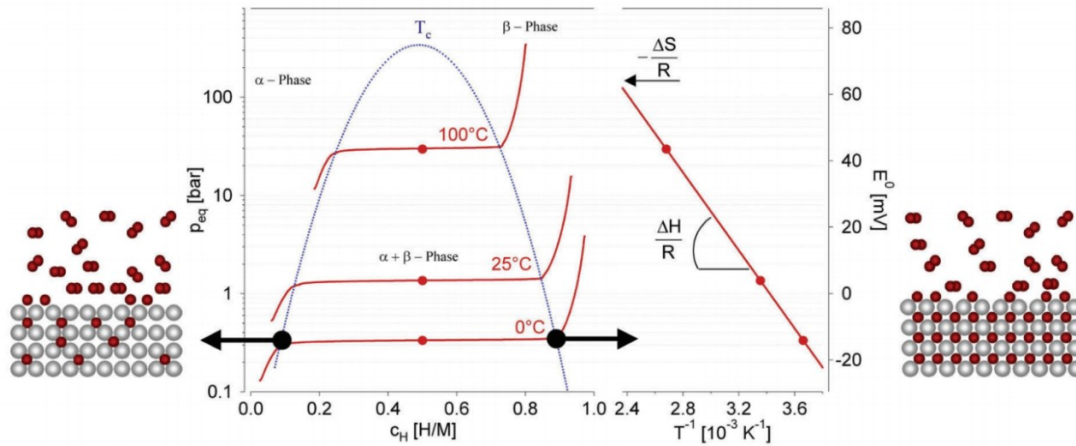
Figure 1.25: Pressure-composition (P-C) isotherms and mechanisms[30]

In Figure 1.25, on the x axis, there is number of H atoms per metal atom, while on the y axis there is pressure of the system. For every different temperature, the length of the plateau determines the amount of hydrogen that can be accommodated reversibly with only a small pressure variation. It is worth to notice that in the first section where cH is below 0.1, hydrogen is present just in the α-phase and the system follows the Sievert's law, expressed by Equation 1.3.7.

$$\frac{H}{M} = kp^0.5 \tag{1.3.7}$$

where k is a constant function of T, $k = k(T)$.

Modified binary hydrides

The most representative compound of this group is magnesium hydride MgH_2, but also AlH_3 and PdH_x have to be mentioned. The interest in the former comes from the high gravimetric capacity (7.66 wt.%) and high abundance on Earth's crust. High gravimetric capacity is beneficial especially in on-board applications because with this storage material the same amount of hydrogen can be stored having a lower material weight, therefore not penalising the performance of the vehicle. However, its formation, see Equation 1.3.8, is not reversible and therefore it needs off-board regeneration.

Magnesium-based metal hydrides are explained in the following section.

$$Mg + H_2 \rightarrow MgH_2 \tag{1.3.8}$$

This reaction occurs at T=850 K and p=200 bar. The ΔH of reaction is -75 kJ mol-1 H_2, which shows the high stability of the compound.

MgH_2 shows a long term cycling stability, up to 2000 cycles.[32] However, in this case, the drawbacks overwhelm the good qualities. MgH_2 has a high desorption temperature (600 K at 1 bar) and unfavourable thermodynamics for mobile applications due to a slow adsorption/desorption mechanism. Furthermore, the kinetics of the pure compound dehydrogenation is too slow. One of the solutions adopted form the late 1990s onwards, in this case, has been mechanical milling and catalytic reaction with Nb2O5. Figure 1.26 represents a comparison of the molecular structure of MgH_2, NaH and LiH.
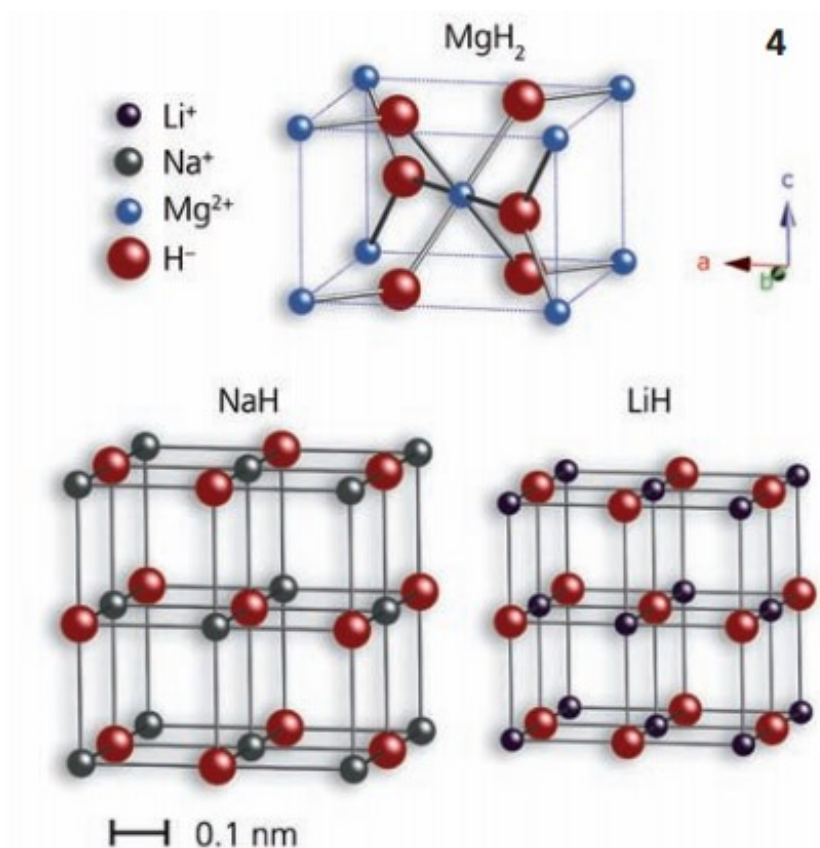
Figure 1.26: Magnesium-based metal hydride and other metal hydrides structures[32]

Complex Hydrides

In this group, hydrogen is bonded with either with ionic or with covalent bonds within the metal. It is possible to further divide them into Alanates and Borohydrides.

Alanates $M(AlH_4)$

This class is made of salts of $[AlH_4]$-. They have been known for many years as potential candidates for hydrogen storage applications due to their high gravimetric capacity. However, they all have high kinetic limits to dehydrogenation/re-hydrogenation in solid form. The situation changed when Bogdanovic and Schwickardi completed a pioneering study on the doping of these hydrides with selected titanium compounds in order to enhance their kinetics.

The most studied compound of this group is certainly $NaAlH_4$. The dehydrogenation reaction of sodium aluminum hydride is a two-step reaction (formation of sodium aluminum hexahydride) shown by Equation 1.3.9 andEquation 1.3.10.

$$3NaAlH_4(7.41wt.\%) \rightarrow Na_3AlH_6 + 2Al + 3H_2(3.7wt.\%H_2 release) \tag{1.3.9}$$

$$Na_3AlH_6(5.9wt.\%) \rightarrow 3NaH + Al + 3/2H_2(1.8wt.\%H_2 release) \tag{1.3.10}$$
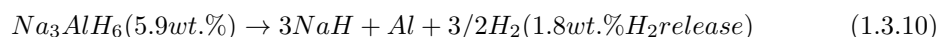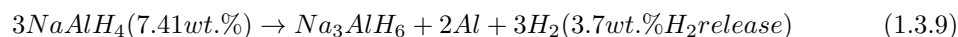
The reaction described by Equation 1.3.9 occurs at 210 – 220 ℃at atmospheric pressure and Ashby and Kobetz[33] have observed its completion in 3 hours. The reaction described by Equation 1.3.10 occurs at around 250 ℃while NaH decomposition does not occur until 425 ℃.

In the 1990s Bogdanovic and Schwickardi determined the consequence of the inclusion of titanium chloride $TiCl_3$ to $NaAlH_4$ on the reversibility of the process. Ti-doped $NaAlH_4$ desorbs hydrogen at around 120 ℃and it can be rehydrogenated at 170 ℃and 15.2 MPa and within 5 hours.[34]

The dehydrogenation rates of hydride doped with TiCl3 were adequate to meet the demands of a fuel cell operating under practical conditions.[28] One critical feature was the effect of cycling of hydrogen load/unload on the material overall capacity. It was found that starting from an initial capacity of 5.6 wt% this property reduced to 4.2% in the second cycle and 3.8% after the third cycle and reduced to 3.1% after 31 cycles.[35,36] This is a negative feature which compromises the potential application of this kind of hydride. The properties of reactions Equation 1.3.8 and Equation 1.3.9 are explained in Table 1.8.

Reaction	Hydrogen (wt% ideal)	Hydrogen (observed) (wt%)		Condition		$\Delta H_{dehydration}$ (kJ/mol H_2)
		1st dehydration	Re-hydration	1st Dehyd. Temp. (℃)	Re-hyd. Temp. (℃) (Press. (MPa))	Exp.
$NaAlH_4$ → NaH + Al + $\frac{3}{2}H_2$	5.6	5.6	5.6	265	27.0 (17.5)	56.5
$NaAlH_4$ → NaH + Al + $\frac{3}{2}H_2$ (with Ti dopant)	5.6	5	3.5-4.3	160	12.0-15-0 (11.5)	56.5

Table 1.8: Properties of reactions[37]

Borohydrides $M(BH_4)$

This group has the highest gravimetric capacity. $Be(BH_4)_2$ is the compound with the highest hydrogen content (more than 20 wt.%), but it is highly toxic. They show a wide operational

29

temperature range: Toperational = 125-350 ℃. However, given this large temperature variation, the release temperature is considered high. In Table 1.9 properties of different borohydrides are compared.

Material	Density (g/mol)	Density (g/cm³)	Hydrogen density (mass%)	Hydrogen density (kg/m³)	T_m (K)	ΔH^f_{boro}
LiBH$_4$	21.78	0.66	18.5	122.1	541	-194
NaBH$_4$	37.83	1.07	10.7	114.5	778	-191
KBH$_4$	53.94	1.17	7.5	87.8	858	-229
RbBH$_4$	100.31	1.92	4.0	76.8	873	-
CsBH$_4$	147.75	2.42	2.7	65.3	873	-
Ca(BH$_4$)$_2$	69.76	1.07	11.6	124.1	533	-302
Al(BH$_4$)$_3$	71.51	0.79	16.9	133.5	208.5	-131

Table 1.9: Basic material properties of borohydrides[31]

From Table 1.9, the alkali metal borohydride $LiBH_4$ has the highest gravimetric capacity (18.5% on mass basis), however reactions Equation 1.3.11 and Equation 1.3.12 have high decomposition temperature, typically between 380 ℃and 500 ℃(the final temperature might depend on the experimental conditions, e.g. the heating rate, the sample preparation, etc.)., i.e. $LiBH_4$ releases hydrogen at 380 ℃, which is a too high temperature for the considered application, whereas LiH decomposition occurs at 727 ℃.

$$LiBH_4 \rightarrow Li + B + 2H_2 \tag{1.3.11}$$

$$LiBH_4 \rightarrow LiH + B + \frac{3}{2}H_2 \tag{1.3.12}$$

where the first step liberates 4.59 wt% and the second step liberates 13.77 wt% (referred to $LiBH_4$ molar mass) of the hydrogen, in the temperature range mentioned above.

$LiBH_4$ is a salt-like, hydroscopic, crystalline material with a reported melting point of 275 ℃and densities of $0.681 gcm^{-3}$ at 25 ℃. At 0 ℃its vapor pressure is much less than 10^{-5} mbar and the salt neither decomposes nor sublimes. Its enthalpy of formation and entropy has been measured and its heat capacity cp was determined from 15 to 303 K.

At 298.16 K the values are: $\Delta H_f = -194.44 kJmol^{-1}, S_0 = 75.91 JK^{-1}mol^{-1}, c_p = 82.60 JK^{-1}mol^{-1}$. Clearly, $LiBH_4$ is too stable for dehydrogenation/hydrogenation cycles on on-board applications and its thermodynamics must be tailored.

Indeed, a research[18] shows the real hydrogen release of $LiBH_4$ to be 12-13 wt% (thermal desorption + ball milling).

Figure 1.27 shows the gravimetric and volumetric H_2 density of most of the currently studied hydrides.

The curved lines at the bottom of the graph show the results (gravimetric and volumetric H_2 densities) for compressed hydrogen storage. The maximum volumetric densities are limited to a maximum of 40 (steel) and 50 (composite material) kg $H_2 m^{-3}$, which respects the 2020 U.S. Department of Energy targets (40 kg $H_2 m^{-3}$), but not the Ultimate technology targets (70 kg $H_2 m^{-3}$). Pressure increases counter-clockwise and the maximum volumetric capacity is reached, with a tradeoff of the following explained parameters, around 100 MPa (steel) and 500 MPa (composite material). Given the different behaviour of the two tank materials, the trend in both cases is constant because the underlining principle is the same: up to a certain point increasing the operating pressure, pure hydrogen density increases and, also, the system density. At a certain pressure though, the specifications of the storage tank have to change because higher pressures require higher lining thicknesses, as explained before. The same trend applies to the gravimetric density which decreases increasing pressure due to the augmented mass of the containing tank. Regarding U.S. Department of Energy gravimetric targets, the 2020 result (5.5 mass%) is obtained for pressures lower than 300 MPa (composite material) and never reached for steel cases. Ultimate target is reached for pressures lower than 150 MPa, which is also a limit point for H_2 volumetric density. The points shown confirm the better performance of the composite material versus the commonly used steel. Physisorption is represented in the curved line above the gaseous H_2 ones.

The above horizontal line in Figure 1.27 indicates the performance of liquid hydrogen storage at 20.3 K. It barely satisfies the Ultimate volumetric storage target, and it does not show any constraint regarding gravimetric hydrogen density since being liquid there is no pressure issue and therefore no demanded high lining thickness variations.

The diagonal lines are system density lines, which are theoretically a linear combination of the x axis and y axis parameter:

$$\frac{g_{system}}{cm^3} = \frac{\frac{kg_{H_2}}{m^3}(y \quad axis)}{\frac{kg_{H_2}}{kg_s system}(x \quad axis)} \cdot 10^{-6} \frac{m^3}{cm^3} \cdot 10^3 \cdot \frac{g_{system}}{kg_{system}} \qquad (1.3.13)$$

This parameter will be paramount in the technical design of the system, especially in the automotive application.

The top-right broken line represents the hydrocarbons hydrogen storage, which, by the way, is not sustainable for the purpose of this thesis. The hydrocarbon complexity decreases shifting rightwards and increasing the gravimetric H_2 density because the percentage of H in the HC molecule increases.

As far as the metal hydrides are concerned, the ones which could meet the 2020 requirements are MgH_2, $NaAlH_4$, KBH_4, $NaBH_4$, $LiAlH_4$, LiH, $Al(BH_4)_3$ and $LiBH_4$. Ultimate targets could be met only by $NaBH_4$, $LiAlH_4$, LiH, $Al(BH_4)_3$ and $LiBH_4$.

Figure 1.28 displays a size comparison of four tanks containing the same amount of hydrogen (4 kg) with different hydrogen storage technologies (compressed H_2 at 200 bar, liquid H_2, $LaNi_5H_6$ and Mg_2NiH_4). According to Sørensen,[38] 4 kg of hydrogen are sufficient for a driving range of over 650 km. More reasonable calculations based on current Toyota Mirai model reveal an equivalent driving range of 400 km.

Figure 1.29 shows a commercial hydrogen storage vessel.
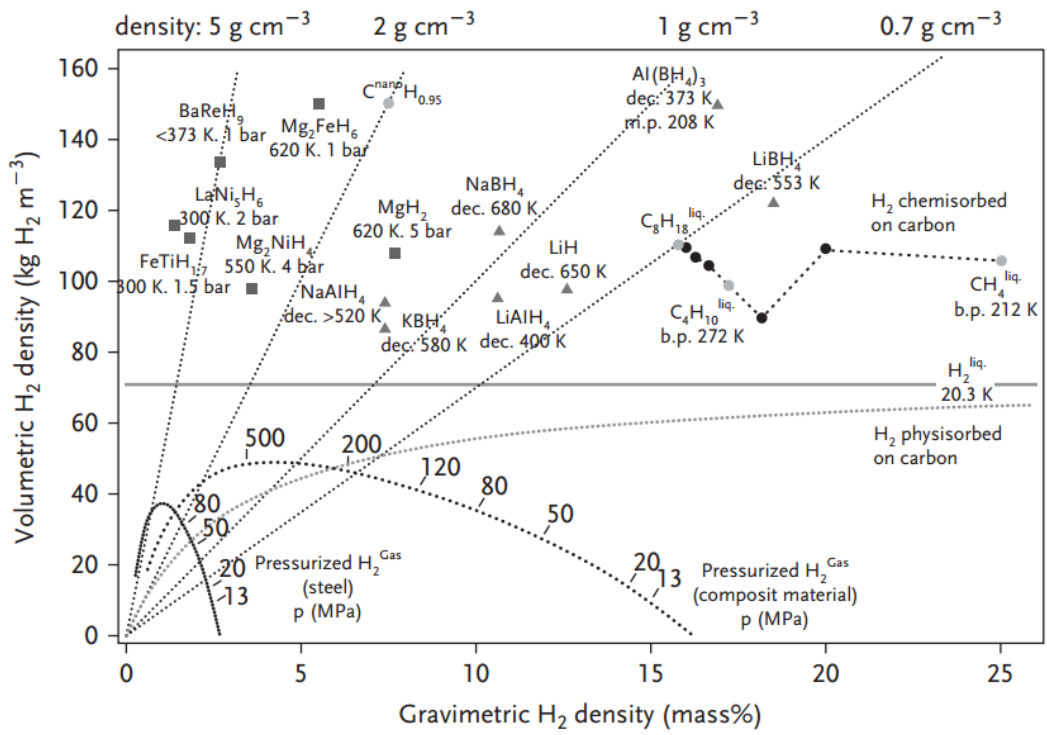
Figure 1.27: Hydrogen storage materials properties (gravimetric and volumetric)[6]

Figure 1.28: Volume of 4 kg of hydrogen stored in different ways[7]
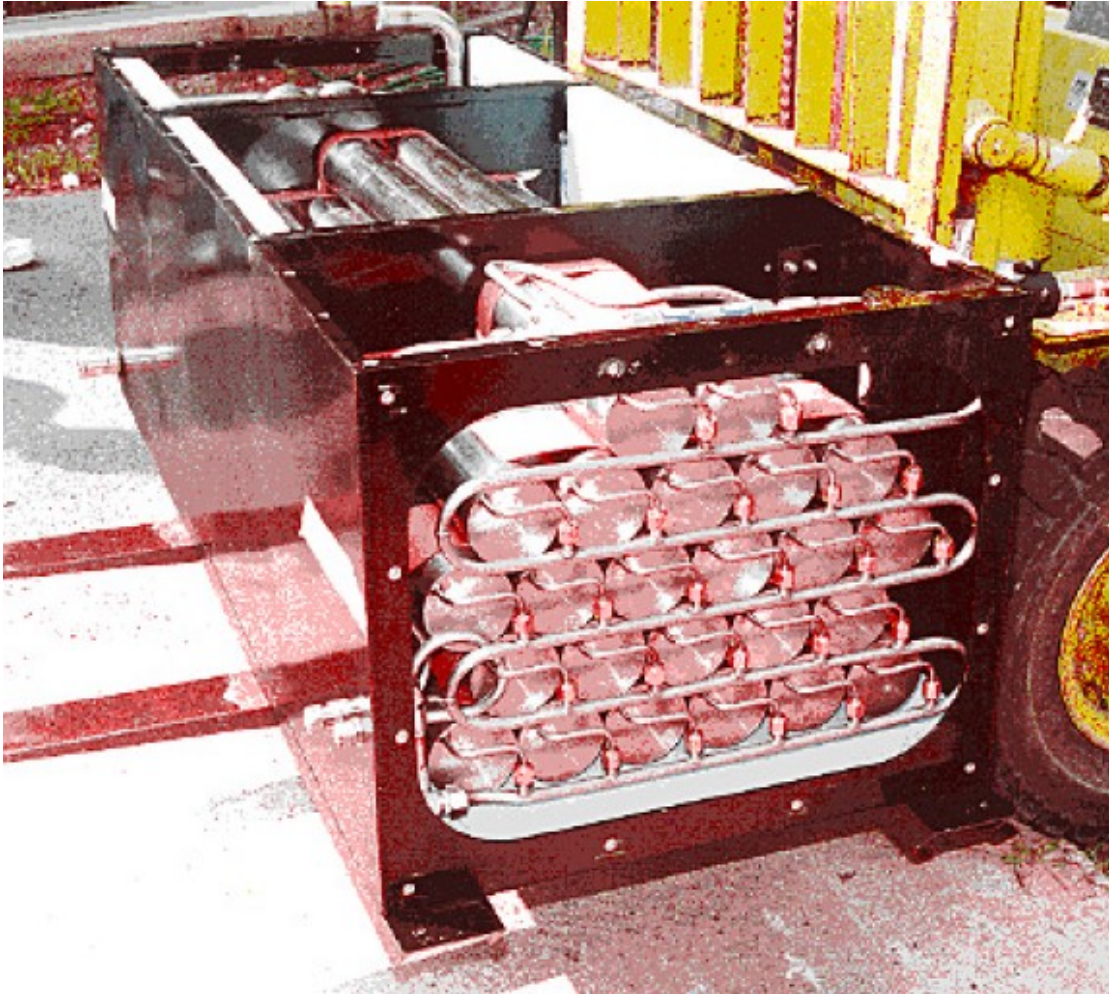
Figure 1.29: Hydrogen storage vessel structure[19]

1.3.3.3 Chemical hydrides: Ammonia

Another method of hydrogen storage is the use of ammonia (NH_3) coming from the Haber-Bosch process, through the reaction Equation 1.3.14.

$$2NH_{3(g)} + 92.4kJ \rightarrow N_{2(g)} + 3H_{2(g)} \qquad (1.3.14)$$
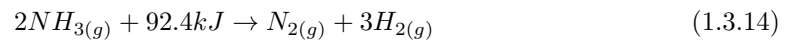
Thermodynamically, 98-99% conversion of ammonia to hydrogen is possible at temperatures as low as 425 ℃. However in practice, the rate of conversion depends on temperature as well as catalysts. According to Cheddie D. 2012, various catalysts have been tested for ammonia decomposition. These include Fe, Ni, Pt, Ru, Ir, Pd, Rh; alloys such as Ni/Pt, Ni/Ru, Pd/Pt/Ru/La; and alloys of Fe with other metal oxides including Ce, Al, Si, Sr, and Zr. Caesium-promoted ruthenium supported on graphite was found to be very promising. For this catalyst, a minimum temperature of 300 ℃is required for efficient release of ammonia for hydrogen production[38]
Ammonia could offer both a short-term solution to the issues of the transportation sector and a long-term, zero-carbon-emission solution with a projected lifetime of two hundred years. Es-

sentially the ammonia economy can achieve the same benefits of a hydrogen economy, but using infrastructure that already exists.

Ammonia is a low-priced basic compound with a boiling point of -33.5 °C at 1 atm and can be stored as a liquid at 8 bar pressure in stainless steel vessels. Ammonia has a very high hydrogen capacity (17.6 wt.% H_2), which can be extracted via thermal catalytic decomposition or electro-oxidation and the hydrogen mass density of liquid ammonia is 1.7 times higher than the hydrogen mass density of pure liquid hydrogen. If we put ammonia on a gravimetric and volumetric H_2 density graph as we did previously, we would obtain the plot in Figure 1.30.
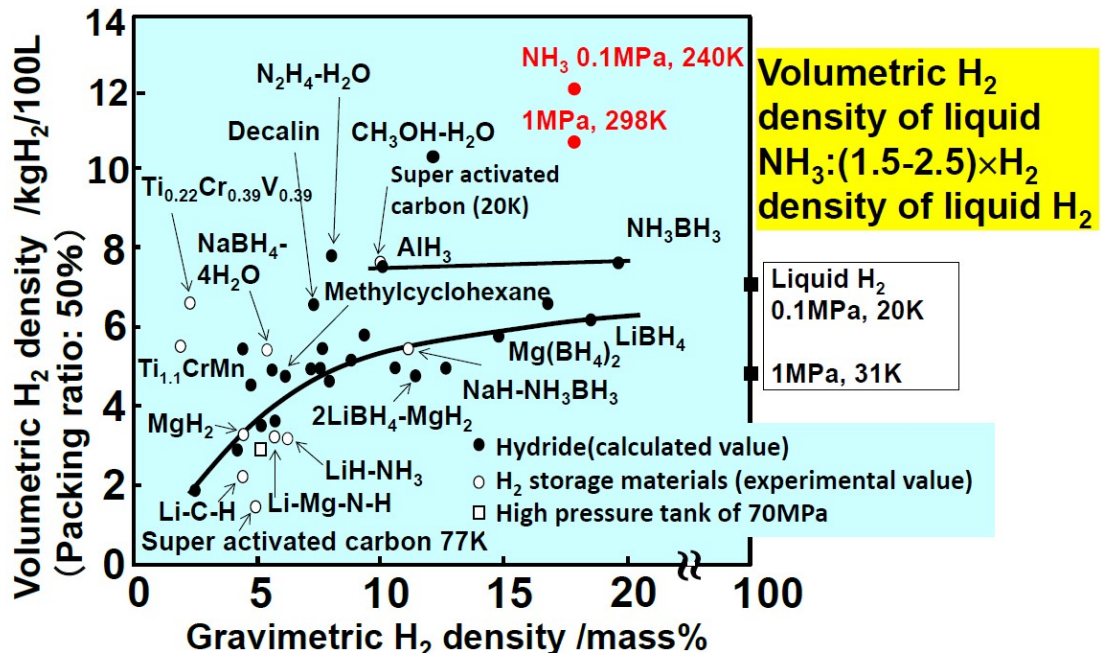
Figure 1.30: NH_3 points on gravimetric H_2 density (x axis) – volumetric H_2 density plot at different thermodynamic conditions[39]

Another advantage of ammonia is its widespread production worldwide and its relatively low price: 131 million tonnes of NH_3 are produced each year worldwide and it was traded at a price of dollar \$310 per metric ton as of the week ending March 4, 2016.[40,41] Table 1.10 explains a cost comparison between ammonia, methanol and hydrogen.

Compound	Total cost ($/kWh)
Ammonia	1.2
Methanol	3.8
Hydrogen	25.4

Table 1.10: Cost comparison[40]

However, its release of hydrogen in an on-board application is not simple due to the thermo-

dynamics of the reaction. Moreover, ammonia gas and liquid can be lethal to human life above certain concentrations by attacking the skin and lungs/respiratory system.

Reaction Equation 1.3.14 is endothermic ($\Delta H_r = +46 \frac{kJ}{molNH_3}$) and therefore it is favoured at high T. Moreover, from the Le Chatelier principle, it can be stated that the reaction is favoured at low pressure. Usually the temperature required is between 300 to 520 ℃ if a Ruthenium catalyst is used.

The theoretical adiabatic efficiency of the reaction is about 85% (on hydrogen LHV basis) because at least 15% of the available energy would have to be burned to supply the heat of reaction.

In the latest years, many different studies have shown that H_2 production can be performed through NH_3 thermal decomposition for small scale fuel cell power systems.[43]

300 ℃ is the minimum temperature in the ammonia decomposition reaction if the ammonia residue has to remain below 2%.

The best catalyst for ammonia decomposition is caesium-promoted ruthenium supported on graphite. For this catalyst, in order to release hydrogen from ammonia a minimum temperature of 300 ℃ is required.

A study[44] found that the best way to reduce the overall costs of on-board fuel cells is to introduce an ammonia cracker and an alkaline fuel cell (AFC), which is able to use the products of the reaction without any purification step.

Literature results

The so-called coupled exothermic and endothermic reactions are similar to what has been done industrially in reactions described as auto-thermal, but to our knowledge, the reactions have not been investigated quantitatively for onboard hydrogen storage materials.

In addition to reducing the amount of heat required for the endothermic reaction, coupling the two reactions also can decrease the maximum temperature generated by the exothermic reaction, thus providing a mechanism to prevent runaway thermal events and/or reduce external cooling requirements.

While exothermic reaction conversion is not limited by hydrogen even at very high pressures, endothermic reaction conversion can be limited by hydrogen partial pressure in the range needed to supply a fuel cell (1 - 5 bar).

The work considered was based on a 43 kWe hydrogen production requirement for automotive applications.

The model predicts the conversion to be 30-40% for both the series and parallel reactions.

These poor conversion levels were due to thermodynamic equilibrium constraints at 5-bar hydrogen.

Chapter 2

Methodology

In order to study the implementation of ammonia for hydrogen storage, a thermodynamics and process analysis was carried out using two types of software: *MTData*™ and *Aspen Plus*™.

2.1 MTData™

MTData™ is a predictive thermochemistry Fortran-written National Physical Laboratory (NPL) software which is a program for the computation of phase equilibria and thermodynamics properties. It is able to compute equilibrium calculations, which was the case analysed in this project.
MTData™ computes the equilibrium results minimising the Gibbs free energy of the system though solution of a non-linear optimisation system with linear constraints.[45]
Given a,b,c,d,... compounds, the free energy can be written as

$$G_s = N_a G_a + N_b G_b + N_c G_c + N_d G_d + \dots \tag{2.1.1}$$

In the studied application the components were just three: H_2, N_2, NH_3 and the phase of each component was gaseous. In MTData™ each compounds studied was categorised as a pure substance.
The equilibrium state of a chemical system is established by solving for a given thermodynamic condition the Equation 2.1.2.

$$MinG = \sum_{j=1}^{N} n_{jj} \tag{2.1.2}$$

Moreover, the constraints explained in Equation 2.1.3 must be respected.

$$\sum_{j=1}^{N} a_{ij} n_j = r_i \tag{2.1.3}$$

$$i = 1, 2, \dots, M \leq N$$
$$n_j \geq 0$$

where

G   Gibbs free energy which is to be minimised by varying the values of the $n_j, j = 1, 2, \ldots, N$

n_j moles of species j

N   number of species within the system

μ_j chemical potential of species j

a_{ji} number of units of component i per species j

M   number of components within the system

r_i number of moles of component i in the system

The advantage of MTData™ is the ability to explore compositions and conditions of pressure and temperature when there are no experimental data.

In this project MTData™ was used to simulate the dehydrogenation of ammonia in an on-board light-vehicle automotive application, see Equation 1.3.14.

It should be pointed out that this sort of analysis regards only the thermodynamics of the reaction since it was not possible to model the kinetics because MTData™ was not suitable for this purpose. Therefore, no information regarding the time of release of hydrogen was discovered and no comparison with the US DoE revised targets for on-board storage of light-duty vehicles have been set. In MTData™ no modelling of the diffusion of NH_3 molecule in a solid catalyst is carried out, but the procedure is a mathematical calculation based on the properties of the input substances.

At first all the databases were imported in the project.

As system components the selected inputs were N_2 and H_2.

After the first step then the program was switched to Multiphase mode because we are dealing with a multiphase mode system. The following conditions were set:

Component ID	Specification	Value
AMMON-01	Split fraction	0
HYDRO-01	Split fraction	0.99
NITRO-01	Split fraction	0
WATER	Split fraction	0
OXYGE-01	Split fraction	0

This was set because, on molar basis, NH_3 is made by 25% of N_2 and 75% of H_2 Then different case studies have been plotted. From the literature it is known that ammonia is stored at ambient temperature at 8 bar pressure, therefore this analysis will have an upper bound of 8 bar. Indeed, the temperature parameter is set at ambient condition (i.e. 25 ℃) in order to

avoid the presence of on-board additional equipment to change the temperature of the ammonia tank, such as heaters or coolers, which could also reduce the overall efficiency of the process. Moreover, since the automotive application is for light vehicle on-board storage, there was an upper bound even for temperature values, which depended on the fuel cells technology adopted, as explained in the following results section. Tests were carried out at pressures of 0.1, 1, 2, 3, 4, 5 and 8 bar.

2.2   Aspen Plus™

In order to simulate better the dehydrogenation reaction of ammonia, Aspen Plus™ software was used. Aspen Plus V8.8™ is a chemical process simulation software used by biochemical and polymers industry for the design, operation and optimisation of processes. It is able to model steady-state processes as desired in the modelling of this project. Aspen Plus™ uses mathematical models to predict the performance of the process.

The process design for the ammonia-cracking reactor has been taken from a US government report.[42]

Gaseous ammonia is flowing through a valve from a storage tank and through and heat exchanger to recover waste heat from hot gases exiting the cracking reactor. The preheated gas would then go through a furnace, which will be modelled in Aspen Plus™ by an heat exchanger with incoming heat flux Q, in order to be heated up to the required temperature of the reaction. The outgoing stream would then be purified in order to obtain pure H_2 (0.99 H_2 molar fraction). The ammonia-cracking process scheme is shown in Figure 2.1.
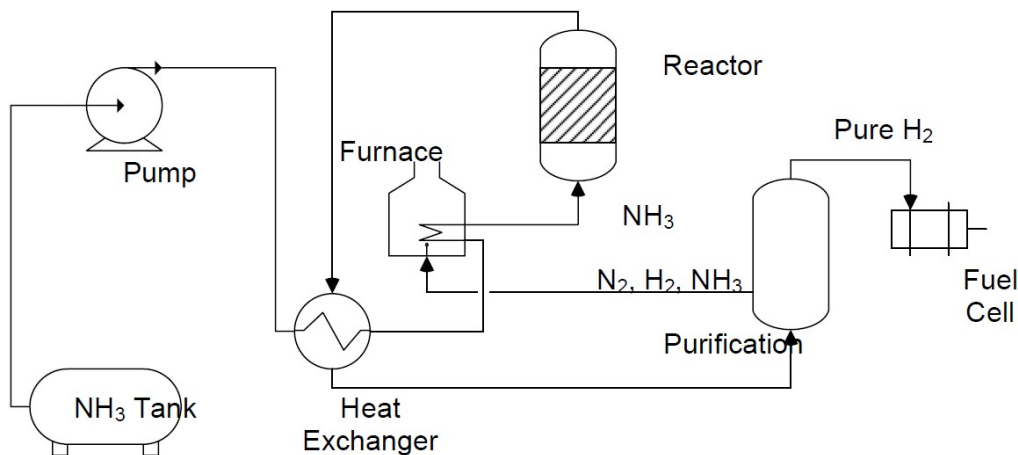
Figure 2.1: Ammonia-cracking process scheme

For on-board storage applications, the reactor would have to work over a very large dynamic span and with very rapid response time to supply a fuel cell. Moreover, it will need to supply enough hydrogen for full power operation of the fuel cell. The full power condition of a 100 kW fuel cell would require 2g/s of hydrogen.[46]

Ammonia and hydrogen exiting as waste stream from the purification reactor could be used in combustion in order to preheat the input stream, through the reactions expressed in Equation 2.2.1 and Equation 2.2.2.

$$2H_2 + O_2 \rightarrow 2H_2O \tag{2.2.1}$$

$$4NH_3 + 3O_2 \rightarrow 2N_2 + 6H_2O \qquad (2.2.2)$$

In the system this combustion would be assimilated to the heat stream incoming in the heat exchanger B3.

At first, the Properties involved have to be specified.

Notice that both water and oxygen were not strictly required for the operations involved, but they would have been required in modelling the combustion processes.

Under *Property Methods & Options* the *Method* filter has been set to *COMMON* (Commonly used property methods) and the *Base method* has been set to *IDEAL* (Ideal property method. It uses both Raoult's law and Henry's law), because the simplest modelling approach has been set for the compounds involved.

Secondly, the *Simulation* of the process had to be set. In particular, the flowsheet diagram was sketched, as shown in Figure 2.2.
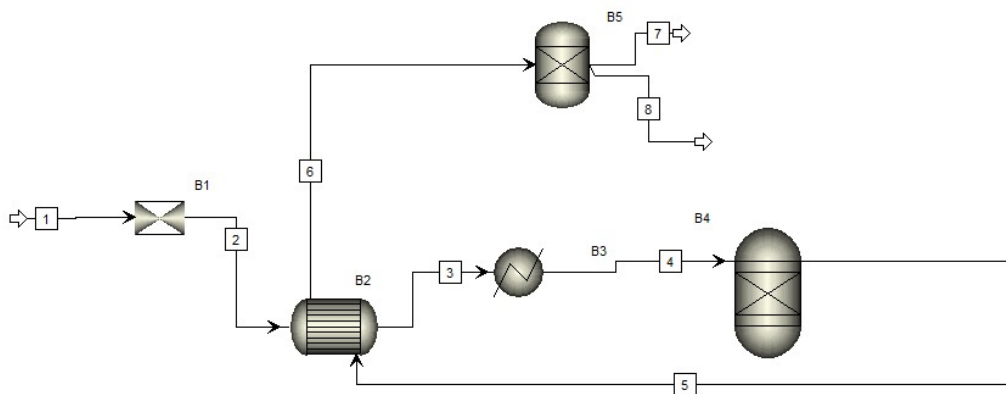
Figure 2.2: Ammonia-cracking process flowsheet

B1 (Valve)
A valve has been selected in order to reduce the pressure of the stream from 8 bar to 1 bar.
Adiabatic flash for specified outlet pressure (pressure changer)
Pressure specification
Outlet pressure: 1 bar
Valid phases: Vapour-Liquid
B2 (HeatX)
This kind of heat exchanger has been selected because it is the most common unit to exchange energy between two fluxes.
Model fidelity: Shortcut
Shortcut flow direction: Countercurrent
Calculation mode: Design
Specification: Cold stream outlet temperature
Value: 100 ℃
B3 (Heater)
This unit has been selected in order to increase the temperature of the feed stream to the temperature required by the endothermic dehydrogenation reaction.
Flash Type: Temperature- Pressure

Temperature: 1000 ℃
Pressure: 1 bar
Valid phases: Vapour-Liquid
B4 (RGibbs)
A Gibbs reactor has been selected because it is used for rigourous reaction and/or multiphase equilibrium based on Gibbs free energy minimisation.
Calculation option: Chemical and physical reaction equilibria
Operating conditions:
    Pressure: 1 bar
    Heat Duty: 0 cal/sec (adiabatic)
Other value were set as default
B5 (Separator)
Outlet stream: 7
Substream: *MIXED*

Physical condition	
Temperature range (℃)	0-1000
Temperature step (℃)	20
Pressure (Pa)	101325
Chemical composition	
x_{N2}	0.25
x_{H2}	0.75

Chapter 3

Results

3.1 MTData™ simulation

The outputs from MTData™ were divided into two groups based on the fuel cell technology adopted, taking into accounts the different operating temperatures:[46, 47]

- A maximum operating temperature of 250 ℃for adopting PEM (Proton Exchange Membrane, which is the most diffused in automotive applications) and AFC (Alkaline Fuel Cells);as a compressed gas;

- A maximum operating temperature of 1000 ℃for adopting SOFC (Solid-Oxides Fuel Cells).

Indeed, the heat of reaction for the dehydrogenation of NH_3 comes directly from the waste heat released by the fuel cell in operation conditions, without any external energy input.

3.1.1 PEM - AFC application
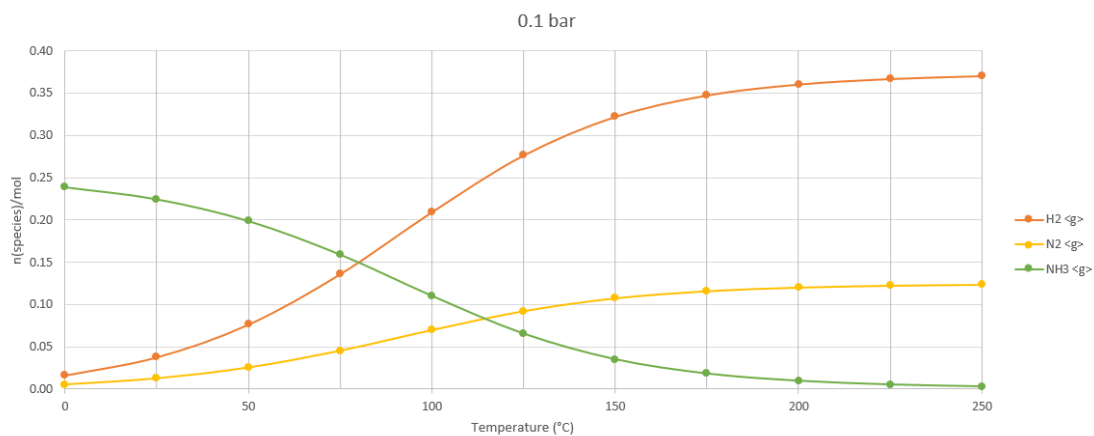
Figure 3.1: Substance amount (n species/mol) - T (℃) plot at 0.1 bar and temperature up to 250 ℃.

In particular, MTData™ output gives information about a range of temperatures of NH_3 decomposition, as shown in Figure 3.1.

If we assumed the reaction to start at 99% and to end at 1% of the initial value of ammonia present in the system, it is possible to put the data in Table 3.1.

The percentage of reaction of N_2 is identical to the H_2 value. Indeed, MTData™ computes in every instant the equilibrium composition among the involved components. Since the input composition is 25% of N_2 and 75% of H_2, the amount of N_2 generated is one third of the amount of H_2 generated at any temperature. However, if we divide the current amount of substance over the final amount of substance for both N_2 and H_2 the same ratio (percentage of reaction) is obtained.

The reaction in Equation 1.3.14 starts at a temperature in between 0 ℃and 25 ℃, as shown in Figure 3.1. If we linearise the function in between this interval, it is possible to compute an approximate temperature at which the reaction reaches 99% of decomposition.

Start Equation 3.1.1 and end Equation 3.1.2 temperature calculations for 0.1 bar pressure and temperature up to 250 ℃:

$$T_{99\%} = \frac{99\% - \%reaction_0}{\frac{\%reaction_{25} - \%reaction_0}{25-0}} + 0 = \frac{0.99 - 1}{\frac{0.940111 - 1}{25-0}} + 0C = 4.17 \tag{3.1.1}$$

$$T_{1\%} = \frac{1\% - \%reaction_{250}}{\frac{\%reaction_{250} - \%reaction_{225}}{250-225}} + 250 = \frac{0.01 - 0.0124}{\frac{0.0124 - 0.02188}{250-225}} + 250 = 256.5 \tag{3.1.2}$$

The reaction ends at a temperature around 250 ℃. If we linearise the function and we extrapolate the value, it is possible to compute the approximate temperature at which the reaction reaches 1%. Notice that linearisation was computed in order to find an approximate value of the start and end temperatures simplifying the nature of the function computed by MTData™, which is shown in Figure 3.1.

Figure 3.2: Substance amount (n species/mol) - T (℃) plot at 1 bar and temperature up to 250 ℃

The reaction in Equation 1.3.14 starts at a temperature in between 0 ℃and 25 ℃, as shown in Figure 3.2. If we apply the linearisation as before the approximate start temperature is 13.5

℃.
The reaction ends after 250 ℃. In this case there is no point in applying extrapolation because the objective percentage (1%) is relatively different from the percentage reached at 250 ℃(10.43%).
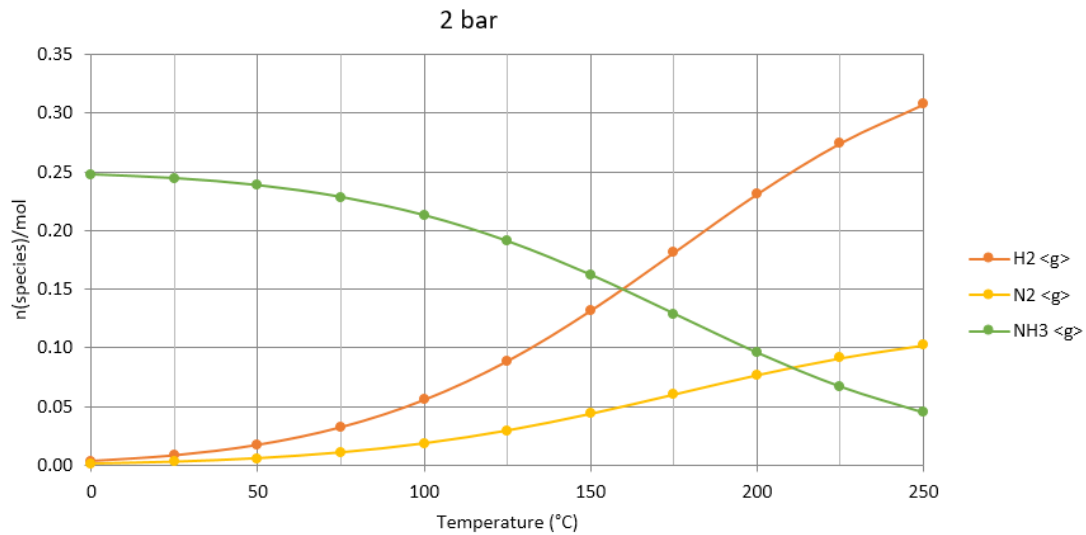
Figure 3.3: Substance amount (n species/mol) - T (℃) plot at 2 bar and temperature up to 250 ℃

The reaction in Equation 1.3.14 starts at a temperature in between 0 ℃and 25 ℃, as shown in Figure 3.3. If we apply the linearisation as before the approximate start temperature is 19.17 ℃.
The reaction ends after 250 ℃. In this case there is no point in applying extrapolation because the objective percentage (1%) is relatively different from the percentage reached at 250 ℃(18.12%).
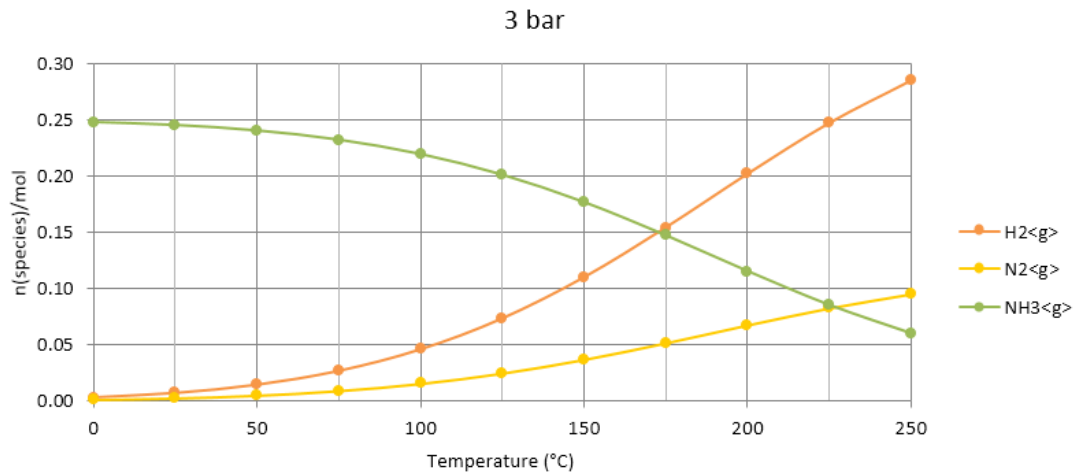
Figure 3.4: Substance amount (n species/mol) - T (℃) plot at 3 bar and temperature up to 250 ℃

The reaction in Equation 1.3.14 starts at a temperature in between 0 ℃and 25 ℃, as shown in Figure 3.4. If we apply the linearisation as before the approximate start temperature is 23.52 ℃.
The reaction ends above 250 ℃. In this case there is no point in applying extrapolation because the objective percentage (1%) is relatively different from the percentage reached at 250 ℃(24.11%).
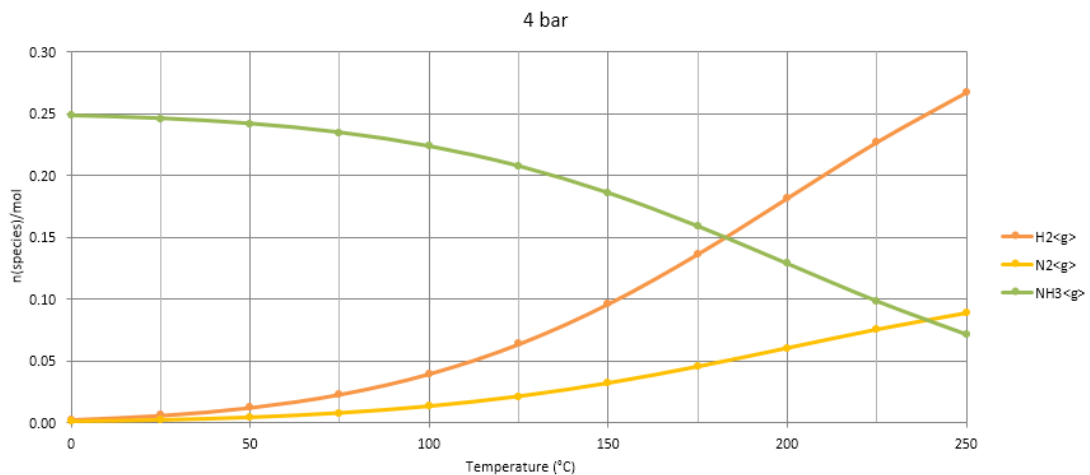
Figure 3.5: Substance amount (n species/mol) - T (℃) plot at 4 bar and temperature up to 250 ℃

The reaction in Equation 1.3.14 starts at a temperature in between 25 ℃and 50 ℃, as shown in Figure 3.5. If we apply the linearisation as before the approximate start temperature is 26.18 ℃.

46

The reaction ends above 250 ℃. In this case there is no point in applying extrapolation because the objective percentage (1%) is relatively different from the percentage reached at 250 ℃(28.95%).
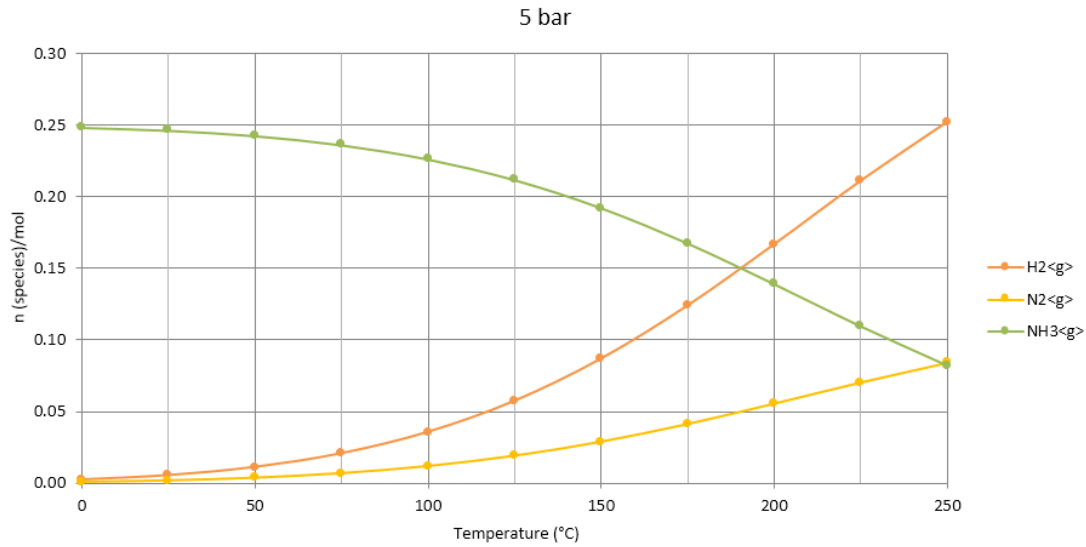
Figure 3.6: Substance amount (n species/mol) - T (℃) plot at 5 bar and temperature up to 250 ℃

The reaction in Equation 1.3.14 starts at a temperature in between 25 ℃and 50 ℃, as shown in Figure 3.6. If we apply the linearisation as before the approximate start temperature is 27.92 ℃.
The reaction ends after 250 ℃. In this case there is no point in applying extrapolation because the objective percentage (1%) is relatively different from the percentage reached at 250 ℃(32.9%).
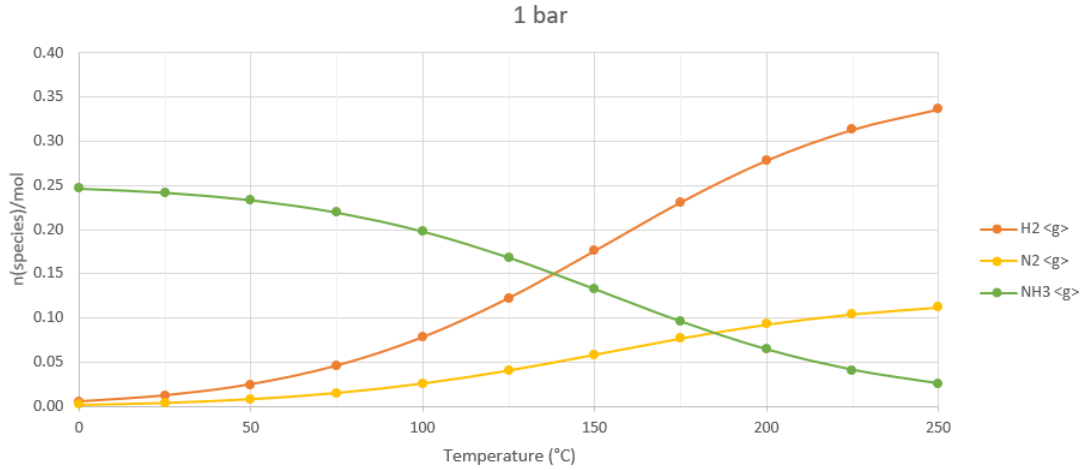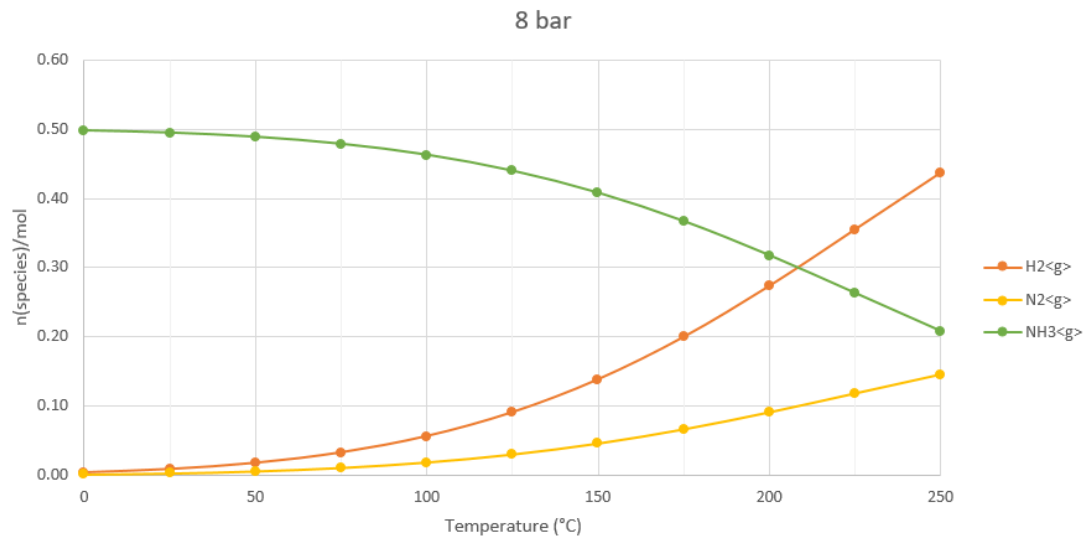
Figure 3.7: Substance amount (n species/mol) - T (℃) plot at 8 bar and temperature up to 250 ℃

The reaction in Equation 1.3.14 starts at a temperature in between 25 ℃and 50 ℃, as shown in Figure 3.7. If we apply the linearisation as before the approximate start temperature is 32.29 ℃.

The reaction ends after 250 ℃. In this case there is no point in applying extrapolation because the objective percentage (1%) is relatively different from the percentage reached at 250 ℃(41.8%).

T (°C)	% Reaction (NH₃ decomposition) 0.1 bar	% Reaction (H₂ formation) 0.1 bar	% Reaction (NH₃ decomposition) 1 bar	% Reaction (H₂ formation) 1 bar	% Reaction (NH₃ decomposition) 2 bar	% Reaction (H₂ formation) 2 bar	% Reaction (NH₃ decomposition) 3 bar	% Reaction (H₂ formation) 3 bar
0	1	0.044	1	0.015	1	0.011	1	0.010
25	0.940	0.102	0.981	0.035	0.986	0.027	0.989	0.024
50	0.832	0.206	0.947	0.073	0.962	0.056	0.969	0.050
75	0.666	0.367	0.890	0.136	0.922	0.105	0.936	0.093
100	0.461	0.565	0.802	0.232	0.859	0.181	0.885	0.160
125	0.274	0.746	0.683	0.363	0.770	0.289	0.810	0.256
150	0.147	0.869	0.538	0.522	0.654	0.428	0.712	0.385
175	0.076	0.938	0.389	0.686	0.521	0.589	0.593	0.540
200	0.040	0.973	0.261	0.827	0.386	0.751	0.464	0.708
225	0.021	0.990	0.166	0.931	0.270	0.892	0.342	0.867
250	0.012	1	0.104	1	0.181	1	0.241	1

Table 3.1: MTData™ output up to 250 ℃(0.1, 1, 2, 3 bar)

T (℃)	% Reaction (NH$_3$ decomposition) 4 bar	% Reaction (H$_2$ formation) 4 bar	% Reaction (NH$_3$ decomposition) 5 bar	% Reaction (H$_2$ formation) 5 bar	% Reaction (NH$_3$ decomposition) 8 bar	% Reaction (H$_2$ formation) 8 bar
0	1	0.009	1	0.009	1	0.008
25	0.990	0.022	0.991	0.021	0.993	0.019
50	0.973	0.046	0.976	0.043	0.981	0.039
75	0.945	0.086	0.950	0.081	0.961	0.074
100	0.900	0.148	0.910	0.140	0.929	0.128
125	0.835	0.238	0.852	0.226	0.883	0.207
150	0.748	0.360	0.773	0.343	0.819	0.316
175	0.640	0.511	0.674	0.490	0.737	0.456
200	0.518	0.680	0.559	0.660	0.638	0.625
225	0.397	0.849	0.440	0.836	0.528	0.812
250	0.289	1	0.329	1	0.418	1

Table 3.2: MTData™ output up to 250 ℃(4, 5, 8 bar)

3.1.2 SOFC application
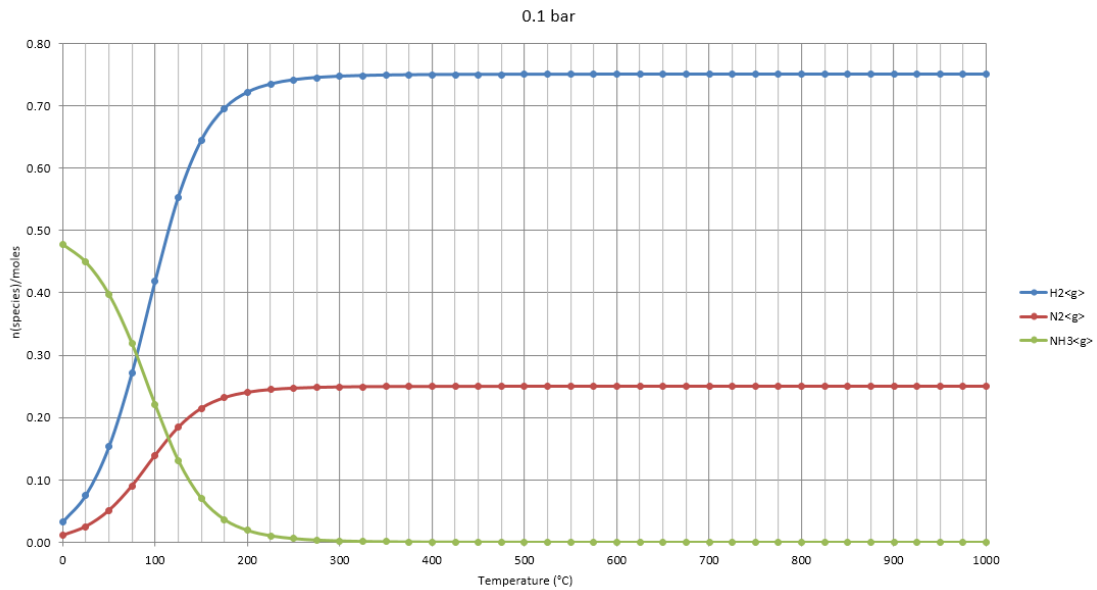
Figure 3.8: Substance amount (n species/mol) - T (℃) plot at 0.1 bar and temperature up to 1000 ℃.

The start temperature of the reaction in Equation 1.3.14 is the same as the case of 0.1 bar and maximum temperature equal to 250 ℃(see Figure 3.1), as shown in Figure 3.8. If we apply the linearisation as before the approximate end temperature is 262.12 ℃.

Moreover, 1 ppm concentration of ammonia is the threshold for the correct functioning of a PEM fuel cell. Therefore, the temperature for obtaining 1 ppm ammonia concentration could be computed through extrapolation with the same procedure used previously in Equation 3.1.1, and it is equal to 1200 ℃.

Figure 3.9: Substance amount (n species/mol) - T (℃) plot at 1 bar and temperature up to 1000 ℃

The start temperature of the reaction in Equation 1.3.14 is the same as the case of 1 bar and maximum temperature equal to 250 ℃(see Figure 3.2), as shown in Figure Figure 3.9. If we apply the linearisation as before the approximate end temperature is 391.78 ℃.

Figure 3.10: Substance amount (n species/mol) - T (℃) plot at 2 bar and temperature up to 1000 ℃

The start temperature of the reaction in Equation 1.3.14 is the same as the case of 2 bar and maximum temperature equal to 250 ℃(see Figure 3.3), as shown in Figure 3.10. If we apply the

linearisation as before the approximate end temperature is 443.3 ℃.
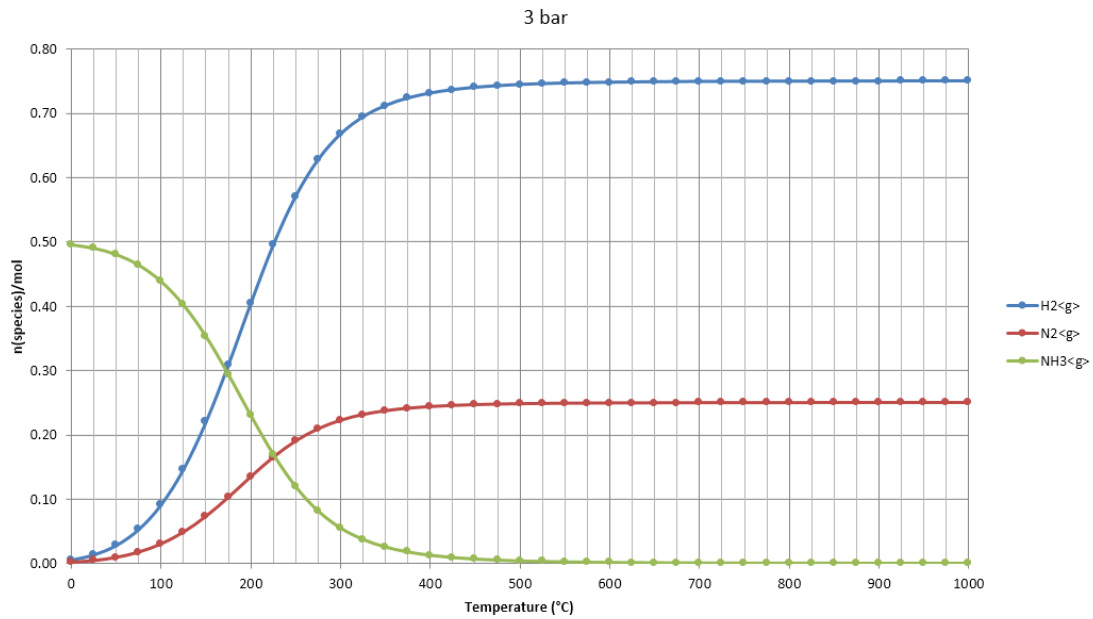
Figure 3.11: Substance amount (n species/mol) - T (℃) plot at 3 bar and temperature up to 1000 ℃

The start temperature of the reaction in Equation 1.3.14 is the same as the case of 3 bar and maximum temperature equal to 250 ℃(see Figure 3.4), as shown in Figure 3.11. If we apply the linearisation as before the approximate end temperature is 476.5 ℃.
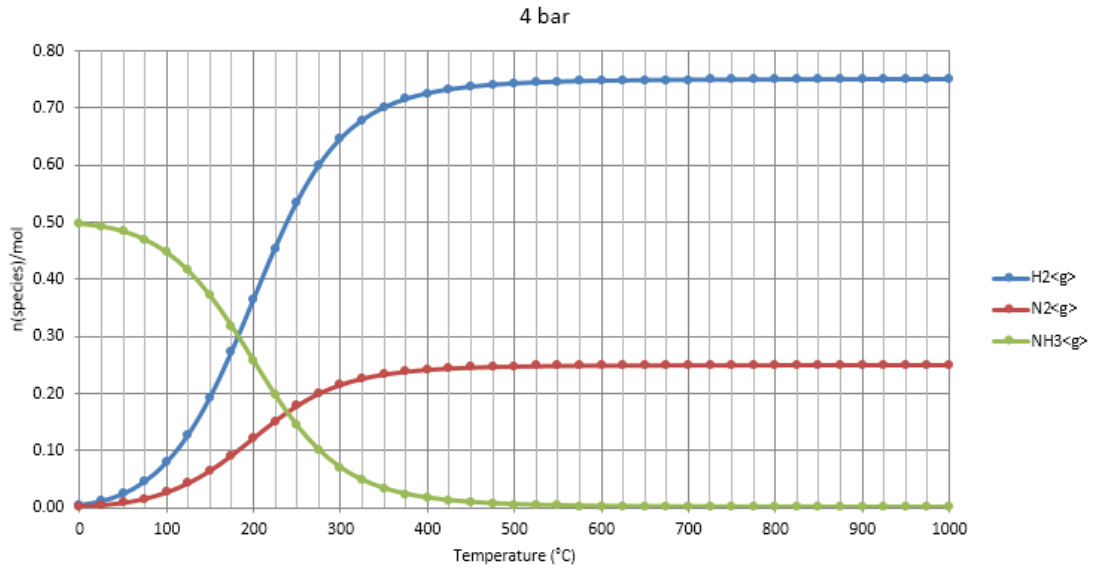
Figure 3.12: Substance amount (n species/mol) - T (℃) plot at 4 bar and temperature up to 1000 ℃

The start temperature of the reaction in Equation 1.3.14 is the same as the case of 4 bar and maximum temperature equal to 250 ℃(see Figure 3.5), as shown in Figure 3.12. If we apply the linearisation as before the approximate end temperature is 502.6 ℃.
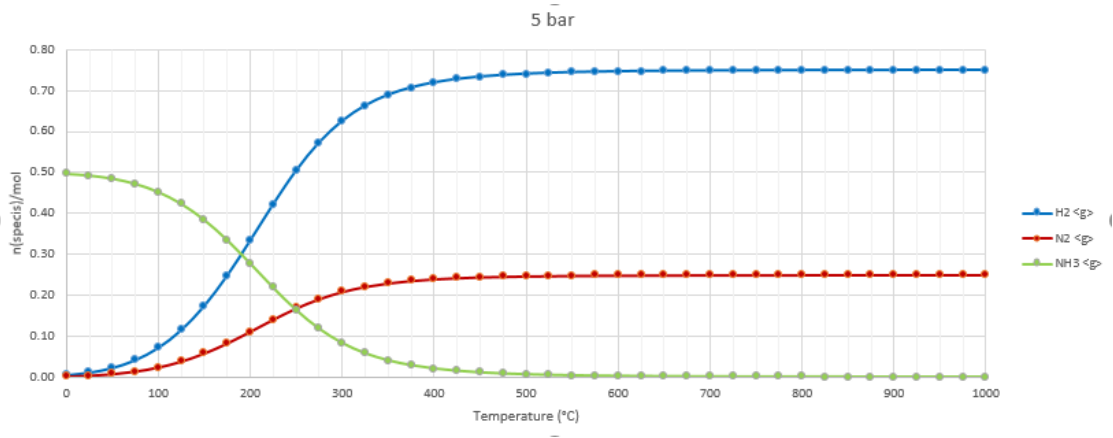
Figure 3.13: Substance amount (n species/mol) - T (℃) plot at 5 bar and temperature up to 1000 ℃

The start temperature of the reaction in Equation 1.3.14 is the same as the case of 5 bar and maximum temperature equal to 250 ℃(see Figure 3.6), as shown in Figure 3.13. If we apply the linearisation as before the approximate end temperature is 523.7 ℃.
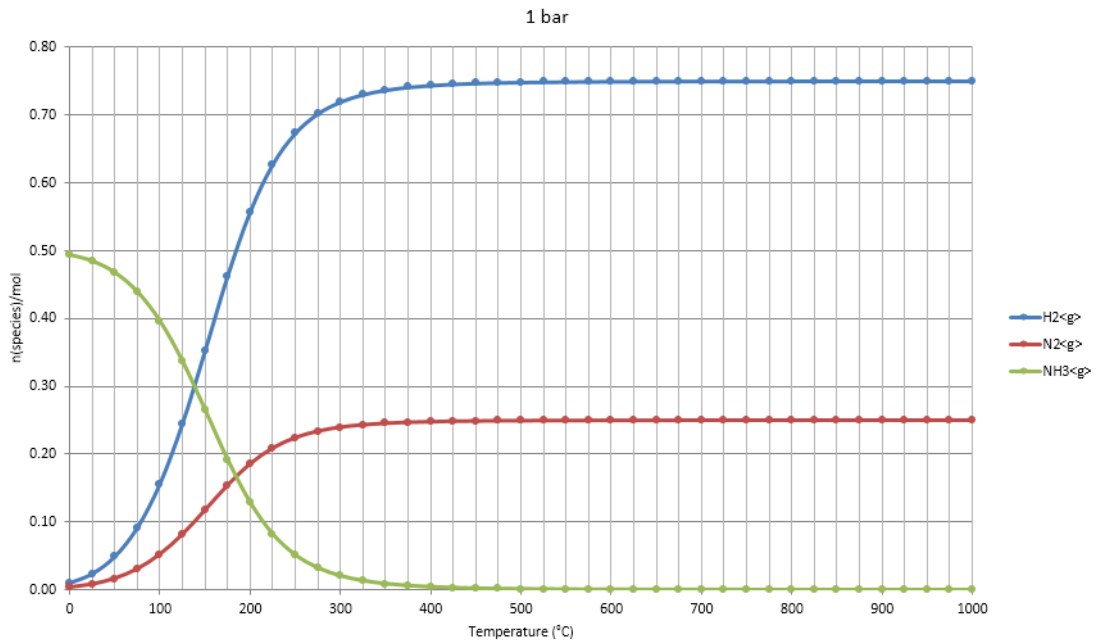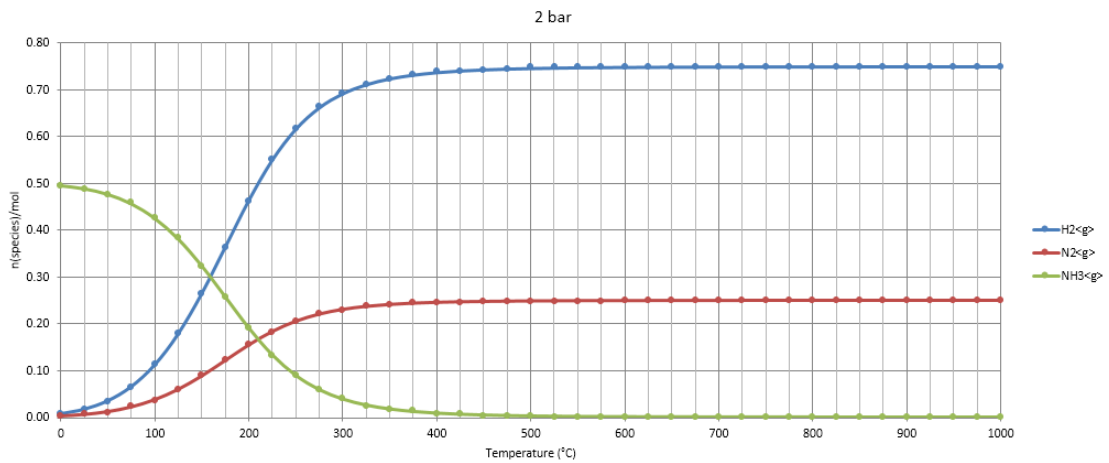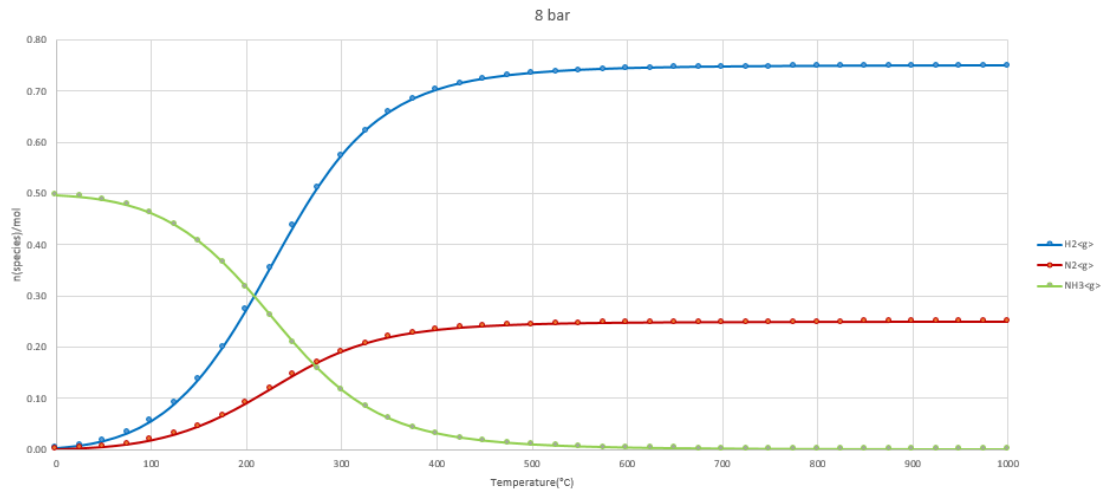
Figure 3.14: Substance amount (n species/mol) - T (℃) plot at 8 bar and temperature up to 1000 ℃

The start temperature of the reaction in Equation 1.3.14 is the same as the case of 8 bar and maximum temperature equal to 250 ℃(see Figure 3.7), as shown in Figure 3.14. If we apply the linearisation as before the approximate end temperature is 572.6 ℃.

T (°C)	% reaction (NH$_3$ decomposition) 0.1 bar	%reaction (H2 formation) 0.1 bar	% reaction (NH$_3$ decomposition) 1 bar	%reaction (H2 formation) 1 bar	% reaction (NH$_3$ decomposition) 2 bar	%reaction (H2 formation) 2 bar	% reaction (NH$_3$ decomposition) 3 bar	%reaction (H2 formation) 3 bar
0	1	0.0436	1	0.0138	1	0.00976	1	0.00797
25	0.940	0.100	0.981	0.0320	0.986	0.0226	0.989	0.0185
50	0.832	0.204	0.947	0.0658	0.962	0.0465	0.969	0.0380
75	0.666	0.362	0.890	0.122	0.922	0.0867	0.936	0.0709
100	0.461	0.558	0.802	0.208	0.859	0.148	0.885	0.122
125	0.274	0.737	0.683	0.326	0.770	0.237	0.810	0.195
150	0.147	0.859	0.538	0.469	0.654	0.351	0.712	0.293
175	0.0762	0.927	0.389	0.615	0.521	0.483	0.593	0.411
200	0.0401	0.961	0.261	0.742	0.386	0.616	0.464	0.539
225	0.0218	0.979	0.166	0.835	0.270	0.732	0.342	0.660
250	0.0124	0.988	0.104	0.897	0.181	0.820	0.241	0.760
275	0.00739	0.992	0.0655	0.935	0.119	0.882	0.164	0.836
300	0.00456	0.995	0.0417	0.958	0.0784	0.922	0.111	0.889

325	0.00291	0.997	0.0272	0.973	0.0522	0.948	0.0753	0.925
350	0.00192	0.998	0.0182	0.982	0.0353	0.965	0.0516	0.949
375	0.00131	0.998	0.0125	0.987	0.0244	0.975	0.0359	0.964
400	0.000915	0.999	0.00877	0.991	0.0172	0.983	0.0255	0.974
425	0.000654	0.999	0.00629	0.993	0.0124	0.987	0.0184	0.981
450	0.000478	0.999	0.00460	0.995	0.00911	0.991	0.0135	0.986
475	0.000356	0.999	0.00343	0.996	0.00681	0.993	0.0101	0.990
500	0.000269	0.999	0.00260	0.997	0.00517	0.995	0.00771	0.992
525	0.000207	0.999	0.00201	0.998	0.00399	0.996	0.00596	0.994
550	0.000162	0.999	0.00157	0.998	0.00312	0.997	0.00466	0.995
575	0.000128	0.999	0.00124	0.998	0.00247	0.997	0.00370	0.996
600	0.000103	0.9999	0.00100	0.999	0.00199	0.998	0.00297	0.997
625	8.39167E-05	0.9999	0.000812	0.999	0.00161	0.998	0.00241	0.997
650	6.88509E-05	0.9999	0.000667	0.999	0.00132	0.998	0.00198	0.998
675	5.70487E-05	0.9999	0.000552	0.999	0.0011	0.999	0.00164	0.998

700	4.77048E-05	0.999	0.000462	0.999	0.000920	0.999	0.00137	0.998
725	4.02319E-05	0.999	0.000389	0.999	0.000776	0.999	0.00116	0.999
750	3.41996E-05	0.999	0.000331	0.999	0.000659	0.999	0.000987	0.999
775	2.92873E-05	0.999	0.000283	0.999	0.000565	0.999	0.000846	0.999
800	2.52549E-05	0.999	0.000244	0.999	0.000487	0.999	0.000729	0.999
825	2.19191E-05	0.999	0.000212	0.999	0.000423	0.999	0.000633	0.999
850	1.91395E-05	0.999	0.000185	0.999	0.000369	0.999	0.000553	0.999
875	1.6808E-05	0.9999	0.000162	0.999	0.000324	0.999	0.000485	0.999
900	1.48397E-05	0.999	0.000143	0.999	0.000286	0.999	0.000428	0.999
925	1.31682E-05	0.999	0.000127	0.999	0.000254	0.999	0.000380	0.999
950	1.17407E-05	0.9999	0.000113	0.999	0.000226	0.999	0.000339	0.999
975	1.05149E-05	0.999	0.000101	0.999	0.000203	0.999	0.000303	0.999
1000	9.45715E-06	1	9.17015E-05	1	0.000182	1	0.000273	1

Table 3.3: MTData™ output up to 1000 ℃(0.1, 1, 2, 3 bar)

T (°C)	% reaction (NH_3 decomposition) 4 bar	%reaction ($H2$ formation) 4 bar	% reaction (NH_3 decomposition) 5 bar	%reaction ($H2$ formation) 5 bar	% reaction (NH_3 decomposition) 8 bar	%reaction ($H2$ formation) 8 bar
0	1	0.00690	1	0.00617	1	0.00488
25	0.990	0.0160	0.991	0.0143	0.993	0.0113
50	0.973	0.0329	0.976	0.0294	0.981	0.0233
75	0.945	0.0614	0.950	0.0550	0.961	0.0435
100	0.900	0.105	0.910	0.0948	0.929	0.0751
125	0.835	0.170	0.852	0.152	0.883	0.121
150	0.748	0.256	0.773	0.231	0.819	0.184
175	0.640	0.364	0.674	0.330	0.737	0.266
200	0.518	0.484	0.559	0.444	0.638	0.365
225	0.397	0.605	0.440	0.562	0.528	0.473
250	0.289	0.712	0.329	0.672	0.418	0.583
275	0.203	0.797	0.237	0.764	0.318	0.683
300	0.140	0.860	0.167	0.833	0.234	0.766

325	0.0968	0.904	0.116	0.884	0.169	0.831
350	0.0671	0.933	0.0818	0.919	0.122	0.879
375	0.0470	0.953	0.0578	0.942	0.0879	0.913
400	0.0335	0.967	0.0414	0.959	0.0638	0.9371
425	0.0243	0.976	0.0301	0.970	0.0468	0.954
450	0.0179	0.982	0.022	0.978	0.0348	0.965
475	0.0134	0.987	0.0167	0.983	0.0263	0.974
500	0.0102	0.990	0.0127	0.987	0.0201	0.980
525	0.00791	0.992	0.00985	0.990	0.0156	0.985
550	0.00620	0.994	0.00773	0.992	0.0122	0.988
575	0.00492	0.995	0.00614	0.994	0.00976	0.991
600	0.00395	0.996	0.00493	0.995	0.00785	0.992
625	0.00321	0.997	0.00401	0.996	0.00639	0.994
650	0.00264	0.997	0.00329	0.997	0.00525	0.995
675	0.00219	0.998	0.00273	0.997	0.00435	0.996

700	0.00183	0.998	0.00228	0.998	0.00364	0.997
725	0.00154	0.998	0.00193	0.998	0.00307	0.997
750	0.00131	0.999	0.00164	0.998	0.00261	0.998
775	0.00112	0.999	0.00140	0.999	0.00224	0.998
800	0.000971	0.999	0.00121	0.999	0.00193	0.998
825	0.000843	0.999	0.00105	0.999	0.00168	0.999
850	0.000736	0.999	0.000919	0.999	0.00146	0.999
875	0.000647	0.999	0.000807	0.999	0.00128	0.999
900	0.000571	0.999	0.000713	0.999	0.00113	0.999
925	0.000507	0.999	0.000633	0.999	0.00101	0.999
950	0.000452	0.999	0.000564	0.999	0.000901	0.999
975	0.000405	0.999	0.000505	0.999	0.000807	0.999
1000	0.000364	1	0.000454	1	0.000726	1

Table 3.4: MTData™ output up to 1000 ℃(4, 5, 8 bar)

Table 3.5, Figure 3.15 and Figure 3.16 summarise the approximate start reaction and end reaction temperatures for every pressure step.

Pressure (bar)	Approximate start reaction temperature (°C)	Approximate end reaction temperature (°C)
0.1	4.17	262.12
1	13.5	391.78
2	19.17	443.3
3	23.52	476.5
4	26.18	502.6
5	27.92	523.7
8	32.29	572.6

Table 3.5: Start reaction Temperature (T) and end reaction T as a function of pressure (p)
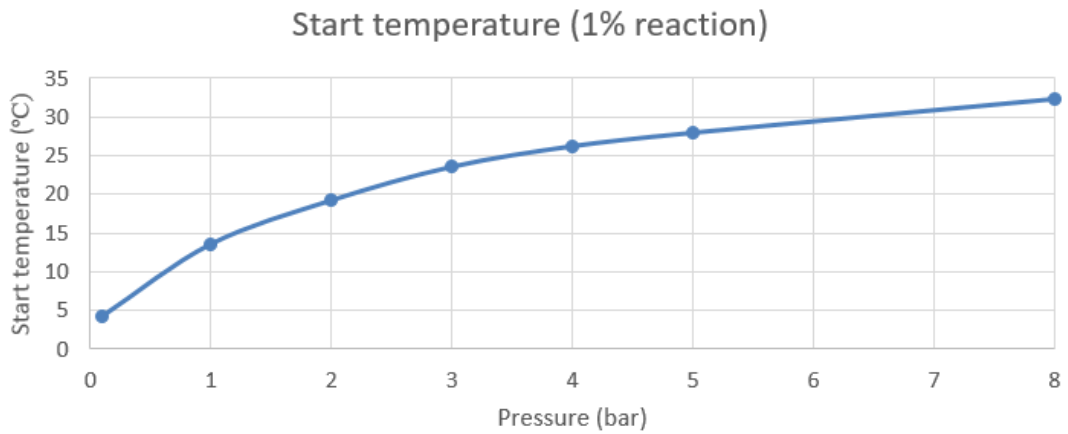

Figure 3.15: Start reaction temperature as a function of p
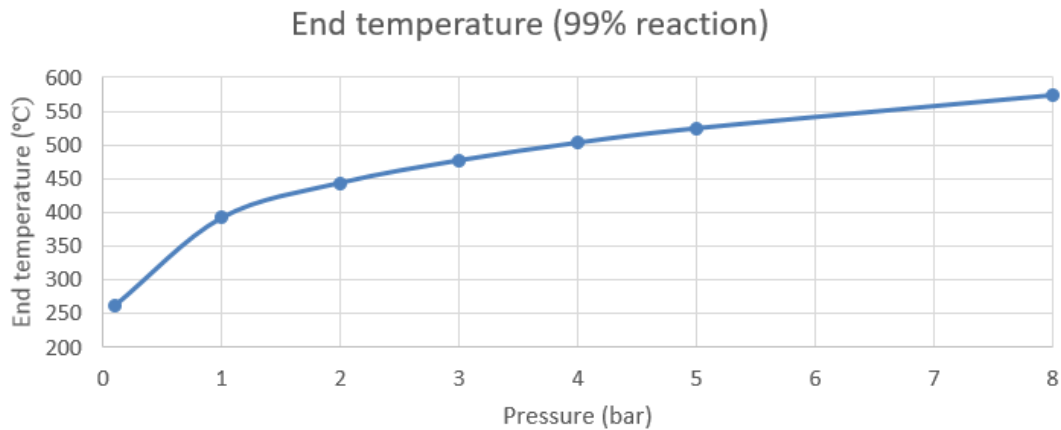
Figure 3.16: End reaction temperature as a function of p

In both the start and end temperature plots, the T(K)-p(bar) profile analised is not linear at the lower pressures (0.1 to 2 bar), whereas it tends to have a constant slope in the upper section (2 to 8 bar). This is due the thermodynamic properties and mechanisms of the reaction and cannot be predicted from theory research without doing software simulations or experiments.
From the feasibility standpoint, there is a significant improvement in lowering the pressure below 2 bar due to this behaviour since the temperature required is much lower than the linear behaviour extrapolation from the upper pressures section.

3.2 Aspen Plus™ simulation

In the Aspen Plus™ simulation, an initial tank of ammonia at 25 ℃(ambient temperature) and 8 bar (stream 1) was connected to the dehydrogenation system with a flowrate of 1 kmol/hr. Subsequently the valve reduced the pressure of the stream to 1 bar (stream 2), before ammonia was injected in the process.
The cold stream outlet temperature of the preheating unit (stream 3) was set at a value of 100 ℃(fixed parameter). Running the simulation the scheme of temperatures and pressure shown in Figure 3.17 was computed:
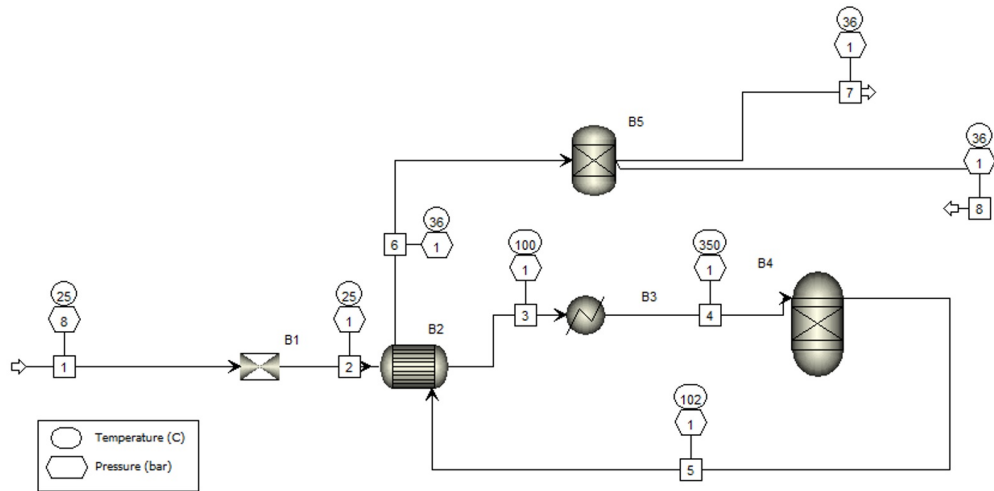
Figure 3.17: Aspen Plus™ simulation flowsheet (T and p indicated)

The heat duty computed at the unit B3 by the system was: 2919.46 J/(sec)or W (nearly 3 kW).

If we scale the process for normal automotive application (100 kW fuel cell), the required flow rate will be 2g/s of H_2:

$$2\frac{g}{s}H_2 = 0.002\frac{kg}{s}H_2 \rightarrow \frac{0.002\frac{kg}{s}}{2.016\frac{kg}{kmol}H_2} = 0.001\frac{kmol}{s}H_2 \qquad (3.2.1)$$

Considering that the output of the process was (stream 7) pure H_2 0.3254 kmol/hr = 0.00009 kmol/s, the heat required would be 32438.44 W or 32.4 kW. This power should come either from combustion of a complementary fuel or coming from waste heat of the fuel cell running the car. Moreover, the maximum temperature reached by the system was 350 ℃(stream 4).

Chapter 4

Discussion and conclusions

The results from the MTData™ simulation confirm that the dehydrogenation of ammonia is endothermic, i.e. the ammonia decomposes increasing the temperature while hydrogen and nitrogen are forming in the ratio 3:1.

The MTData™ outputs confirm the Le Châtelier principle that the reaction is favoured at low pressures so that as pressure increases, the temperature range at which the reaction is occurring should rise.

Moreover, the output from MTData™ simulation can be compared with the results found in the literature.[42]

Temperature (°C)	Unconverted NH₃ 1 bar (HSC Chemistry 4.0 Program, Outokumpu Research Oy, Pori, Finland)[21]	Unconverted NH₃ 1 bar (MTData™ output)
400	0.88 %	0.877 %
500	0.26 %	0.260 %
600	0.10 %	0.100 %
700	0.047 %	0.046 %
800	0.025 %	0.024 %
900	0.015 %	0.014 %

Table 4.1: Equilibrium ammonia conversion

Table 4.1 shows how the simulation and the literature results are the same. Literature results were obtained with a different software called HSC ChemistryTM, which is a chemical reaction and equilibrium program as MTData™,with a versatile flowsheet simulation module. HSC is designed for various kinds of chemical reactions and equilibria calculations as well as process simulation. Therefore, this provides confidence in the results of the simulation. However, MT-Data™ software is not suitable for modelling the kinetics of the reaction and the complex gas-solid interactions in case of insertion of a solid catalyst to enhance the reaction, which would be likely present in its implementation in a real-world process.

The literature reference results for 10 bar could not have been checked because the maximum operating pressure was 8 bar.

For completeness of information, Table 4.2 shows a comparison between the results for 10 bar and the simulation results for 8 bar:

Temperature (°C)	Unconverted NH₃ 10 bar (HSC Chemistry 4.0 Program, Outokumpu Research Oy, Pori, Finland)[21]	Unconverted NH₃ 8 bar (MTData™ output)
400	7.91 %	6.383 %
500	2.55 %	2.013 %
600	1.00 %	0.785 %
700	0.47 %	0.364 %
800	0.25 %	0.193 %
900	0.15 %	0.113 %

Table 4.2: Equilibrium ammonia conversion

Pressure (bar)	Approximate start reaction temperature (°C)	Approximate end reaction temperature (°C)
0.1	4.1	262.1
1	13.5	391.7
2	19.1	443.3
3	23.5	476.5
4	26.1	502.6
5	27.9	523.7
8	32.3	572.6

Table 4.3: Start reaction T and end reaction T as a function of p

However, looking at the results summarised in Table 4.3, it can be deduced that using PEM or AFC technologies to preserve the reaction is not a feasible option because the maximum allowed temperature (250 ℃) is not enough to complete the dehydrogenation even for the most favoured case (pressure = 0.1 bar). Furthermore, the Aspen Plus™ simulation confirms this because the

computed maximum temperature of the stream 3 to make the reactor run properly is 350 ℃. The simulation suggested also the necessity of a power source of 32438.44 W or 32.4 kW for a real system. This result makes the application difficult to implement because the amount of heat required is in the same order of magnitude of the power the fuel cell fed (100 kW). Accordingly the three suggested alternatives for running an on-board dehydrogenation of ammonia are:

- Using a SOFC which has an operating temperature around 1000 ℃, which could sustain the reaction;

- Utilizing an internal combustion system (running on complementary fuel such as gasoline or diesel) to sustain the reaction;

- Installing a battery system able to provide the required heat at the specific temperature (400 ℃ in the 1 bar case).

The whole process has been modelled considering the idealised scenario, however real-world decomposition conditions involve tradeoffs between the soaring operating costs at higher temperatures and removal costs of unconverted NH_3.

In particular, from the previous data, the limit of 1 ppm unreacted ammonia was nearly reached at pressure equal to 0.1 bar and 1200 ℃ which are unfeasible for the purpose of this project and for real life scenarios due to the very high temperature required, and maybe reached only in a stationary application. Moreover, at high temperatures (1000 ℃), hydrogen strongly attacks the stainless steel and makes it brittle. This is due to the high temperatures which increase hydrogen solubility within the metal. Hydrogen diffusion in the metal weakens its structure and subsequently generates fractures. Regarding the aims and objectives of the project, ammonia as chemical hydrogen storage mean has been confirmed to be a promising technology. H_2 properties make hydrogen the ideal, clean replacement of current fuels such as petrol and diesel. Nevertheless, some critical features such as heat management and safe handling of ammonia reaction have been discovered. Moreover, the interesting ammonia to hydrogen decomposition has been modelled only in the ideal way, not accounting for the kinetics and, therefore, the timing of the process, which is paramount in the automotive application, since vehicles have to be run safely and uninterruptedly.

In conclusion, neither of the used software was able to model the real reaction properly, because, at present, making hydrogen from ammonia relies on ruthenium as a catalyst. This Ru-based catalyst require a minimum temperature of 300 ℃ for efficient release of ammonia for hydrogen production. It is widely agreed that Ru is the best catalyst for decomposition at 400 ℃, while Ni based catalysts perform comparably at 600 ℃.

Ruthenium is a precious and expensive metal, and the process to separate the hydrogen requires extreme temperatures. But using the sodium-based process proposed by British scientists Martin Owen Jones and Bill David, the process would require temperatures of only 400 degrees Celsius; a typical car battery could supply enough energy to heat their small reactor to that temperature. The output of their device is not enough to power a large commercial operation, but could be scaled up to supply hydrogen to a fuel cell for cars.[47,48] The MTData™ results confirm the theory on the potential of ammonia in hydrogen economy. The most critical feature of the process remains the supply of heat to the reaction in the most economical and safe condition. Simply stated, most of the performance parameters of ammonia reactors would need at least two orders of-magnitude improvements in order to be used on-board commercially viable hydrogen powered fuel cell vehicles. In comparison, metal hydrides seem to be a suitable alternative, but their potential needs to be proven at R&D stage.

Chapter 5

Future work

This work gives a cursory estimate of the requirements for hydrogen production from ammonia, but a more comprehensive well-to-wheels analysis of ammonia production, distribution, and use is needed. The analysis should include the production of ammonia from feedstocks other than natural gas, including renewables.

For the future of hydrogen storage, enhancement of the capacity and release properties of the existing metal hydrides is required. In particular, looking at Figure 1-10 the most promising materials which are respecting the US DoE 2015 target are $Al(BH_4)_3$, $NaBH_4$, $LiBH_4$ and $LiAlH_4$. New R&D studies are needed also for ammonia dehydrogenation reaction, mainly to solve heat management in a cost-efficient way and to improve the kinetics using catalysts, among which Platinum-Group metal surface seems to be the most feasible option.

Especially interesting are organic liquids with considerable hydrogen storage capacity (HSC), which can be easily handled and transported, using the existing infrastructure of the oil or gasoline industry.

The cutting-edge technology in hydrogen storage regards new nanoporous materials which can achieve US DoE future targets and store hydrogen efficiently and economically in a hydrogen energy-driven future.

Bibliography

[1] (2015), United Nations, Department of Economic and Social Affairs, Population Division. World Population Prospects: The 2015 Revision. (Medium variant), *Population Pyramids of the World from 1950 to 2100*, available at:
`http://populationpyramid.net/world/2030/`

[2] (2015), UN projects world population to reach 8.5 billion by 2030, driven by growth in developing countries, available at:
`http://www.un.org/sustainabledevelopment/blog/2015/07/un-projects-world-population-to-reach-8-5-billion-by-2030-driven-by-growth-in-developing-countries/`
(July 29th, 2015)

[3] S. Solomon, D. Qin, M. Manning, Z. Chen, M. Marquis, K. Averyt, M. Tignor, and H. Miller, IPCC 2007: *Technical summary, Climate Change 2007: The Physical Science Basis. Contribution of Working Group I to the Fourth Assessment Report of the Intergovernmental Panel on Climate Change*, 2007.

[4] (2016), *Fast facts, International Energy Agency*, available at:
`http://www.iea.org/topics/transport/`

[5] IEA (International Energy Agency) (2015) '*Technology Roadmap - Hydrogen and Fuel Cells*'

[6] Godula-Jopek A., Jehle W., Wellnitz J. (2012), "*Hydrogen – Fundamentals*" in: Wiley-VCH Verlag GmbH & Co. KGaA (editors), *Hydrogen Storage Technologies, New Materials, Transport and Infrastructure*, p.11-79

[7] Singh S., (2009), *Hydrogen Storage in Nanostructured Light Metal Hydrides*, Master of Science in Physics, Indian Institute of Technology Madras Geboren te Haridwar, India, Delft University of Technology, Delft.

[8] (2008), *Fuel Cell School Buses Report to Congress*, Section 743(c) of Public Law No. 109-58, US Department of Energy

[9] Godula-Jopek A., Jehle W., Wellnitz J. (2012), "*Hydrogen Application: Infrastructural Requirements*" in: Wiley-VCH Verlag GmbH & Co. KGaA (editors), *Hydrogen Storage Technologies, New Materials, Transport and Infrastructure*, p.81-96

[10] U.S. Department of Transportation, Bureau of Transportation Statistics, Omnibus Household Survey. (October 2003). "*From Home to Work, the Average Commute is 26.4 Minutes*", available at: https://en.wikipedia.org/wiki/Charging_station
(accessed 8th August 2016)

[11] (2009), The National Hydrogen Association, available at:
http://www.hydrogenassociation.org/general/factSheets.asp

[12] (1945), *Notes by J B S Haldane on Mixtures of Hydrogen and Air*, Copyright UCL 2014, available at:
http://archives.ucl.ac.uk/DServe/dserve.exe?dsqIni=Dserve.ini&dsqApp=Archive
&dsqDb=Catalog&dsqCmd=NaviTree.tcl&dsqField=RefNo&dsqItem=HALDANE/4/16/1/39
#HERE

[13] (2003) Jeremy Rifkin, *Hydrogen Economy*, Penguin Group (USA), New York

[14] Ball M. and Wietschel M. (2009), *The Hydrogen Economy Opportunities and Challenges*, Cambridge University Press, Cambridge, UK

[15] P. Hoffmann., (2002), *Tomorrow's energy: Hydrogen, fuel cells, and prospects for a cleaner planet.* The MIT Press, Cambridge, Massachusetts

[16] Nuno Maria Marques dos Santos Bimbo (2013), *Modelling and Analysis of Hydrogen Storage in Nanostructured Solids for Sustainable Energy Systems* (Ph.D. thesis), University of Bath

[17] Klell, M. (2010), '*Storage of Hydrogen in the Pure Form*'

[18] Hydrogen storage, U.S. Department of Energy, available at:
http://energy.gov/eere/fuelcells/hydrogen-storage

[19] Hirscher M. (2010), *Handbook of Hydrogen Storage New Materials for Future Energy Storage*, WILEY-VCH Verlag GmbH & Co. KGaA, Weinheim

[20] Eberle, U., Felderhoff, M., & Schüth, F. (2009). *Chemical and Physical Solutions for Hydrogen Storage.* Angewandte Chemie-International Edition, 48, 6608-6630.

[21] A. Zuttel, A. Remhof, A. Borgschulte, and O. Friedrichs, "*Hydrogen: the future energy carrier*" Philosophical Transactions of the Royal Society London, Series A (Mathematical, Physical and Engineering Sciences), vol. 368, no. 1923, pp. 3329-3342, 2010.

[22] Gray, H.R. and Joyce, J.P. (1976) 'Hydrogen environment embrittlement of turbine disk alloys', (March)

[23] Gillette, J. and Kolpa, R. (2007) 'Overview of Interstate Hydrogen Pipeline Systems', pp. 1–3.

[24] Herring, D.H. (2010) 'Hydrogen embrittlement.', Wire Forming Technology International, , pp. 1–4.

[25] Practice, G. and Control, C. (2000) 'Stress Corrosion Cracking', National Physical Laboratory

[26] Murakami Y. and Matsuoka S. - Effect of hydrogen on fatigue crack growth of metals - Engineering Fracture Mechanics, Vol. 77, Issue 11, 2010, Pages 1926-1940

[27] Capelle J., Gilgert J., Pluvinage G. - Hydrogen effect on fatigue and fracture of pipelines - Paper presented at the conference ICMFM XIII, 2006.

[28] 'Corrosion resistance', available at:
http://www.outokumpu.com/en/products-properties/more-stainless/corrosion-resistance/Pages/default.aspx#top

[29] Dornheim, M. (2011) 'Thermodynamics of Metal Hydrides : Tailoring Reaction Enthalpies of Hydrogen Storage Materials', Thermodynamics - Interaction Studies - Solids, Liquids and Gases, Dr. Juan C, pp. 891–918.

[30] Broom, Darren P. (2011), *Hydrogen Storage Materials The Characterisation of This Storage Properties*, Springer-Verlag London Limited, London

[31] Zuttel, A. (2003) *Materials for hydrogen storage*, Materials Today, 6(9), pp. 24–33.

[32] Z. Dehouche, R. Djaozandry, J. Huot, S. Boily, J. Goyette, T.K. Bose, and R. Schulz., (2000), *Influence of cycling on the thermodynamic and structure properties of nanocrystalline magnesium based hydride.* J. Alloy. Compd., 305:264

[33] E.C. Ashby, P. Kobetz, *Inorganic Chemistry*, 1966

[34] G.D. and Zatti, M. (2011) '*Engineering Transition Metal Borohydrides for Energy Storage and Conversion*' (MSc thesis), Politecnico di Milano

[35] B. Bodganovic, M. Schwickardi. *J. Alloy Comp*, 1997, 253-254

[36] Walker G. (2008), *Solid-state hydrogen storage Materials and chemistry*, Woodhead Publishing Limited, Cambridge, England

[37] Ragheb, M. (2011), *Hydrides alloys for hydrogen storage*, available at:
`http://mragheb.com/NPRE%20498ES%20Energy%20Storage%20Systems/Metal%20Hydrides`
`%20Alloys%20for%20Hydrogen%20Storage.pdf`

[38] Sørensen B. (2012), *Hydrogen and Fuel Cells*, Elsevier Ltd., Oxford, UK

[39] Kojima, Y. (2014) '*Liquid Ammonia for Hydrogen Storage*', (September)

[40] (2015), '*Hydrogen From Ammonia – Will It Work?*' available at:
`http://gas2.org/2015/04/28/hydrogen-from-ammonia-will-it-work/`

[41] Did, H. et al. (2016) 'Ammonia Prices Fell Slightly from the Previous Week', pp. 1–2, available at:
`http://marketrealist.com/2016/03/weekly-ammonia-price-update-week-ending`
`-march-4-2016/`
`(accessed on 8th August 2016)`

[42] Thomas, G. and Parks, G. (2006), *Potential Roles of Ammonia in a Hydrogen Economy*, U.S. Department of Energy, pp. 1–23.

[43] Wang, W. et al. (2013), *Ammonia as hydrogen carrier for transportation; Investigation of the ammonia exhaust gas fuel reforming*, International Journal of Hydrogen Energy, 38(23), pp. 9907–9917.

[44] Kordesch, K. et al. (2003), *Ammonia as Hydrogen Source for an Alkaline Fuel Cell – Battery Hybrid System*, Technical University Graz, pp. 1–4.

[45] Davies, R.H. et al. (2002), *MTDATA-thermodynamic and phase equilibrium software from the national physical laboratory*, Calphad, 26

[46] Types of fuel cells, U.S. Department of Energy, available at:
`http://energy.gov/eere/fuelcells/types-fuel-cells` (accessed on 8th August 2016)

[47] (2009), The National Hydrogen Association, available at:
http://www.hydrogenassociation.org/general/factSheets.asp

[48] (2013), *Airliquide Gas Encyclopedia*, available at:
http://encyclopedia.airliquide.com/Encyclopedia.asp?GasID=36#GeneralData
(accessed on 9th August 2016)